

UNIVERSIDAD DE CONCEPCIÓN



CENTRO DE INVESTIGACIÓN EN
INGENIERÍA MATEMÁTICA (CI²MA)



Non-conforming/DG coupled schemes for multicomponent
viscous flow in porous media with adsorption

RAIMUND BÜRGER, SUDARSHAN K. KENETTINKARA,
RICARDO RUIZ-BAIER, HECTOR TORRES

PREPRINT 2017-08

SERIE DE PRE-PUBLICACIONES

NON-CONFORMING/DG COUPLED SCHEMES FOR MULTICOMPONENT VISCOUS FLOW IN POROUS MEDIA WITH ADSORPTION*

RAIMUND BÜRGER[†], SUDARSHAN K. KENETTINKARA[‡], RICARDO RUIZ-BAIER[§],
AND HECTOR TORRES[¶]

Abstract. Polymer flooding is an important stage of enhanced oil recovery in petroleum reservoir engineering. A model of this process is based on the study of multicomponent viscous flow in porous media with adsorption. This model can be expressed as a Brinkman-based model of flow in porous media coupled to a system of non-strictly hyperbolic conservation laws having multiple components. The discretisation proposed for this coupled flow-transport problem combines a stabilised non-conforming method for the Brinkman flow problem with a discontinuous Galerkin (DG) method for the transport equations. The DG formulation of the transport problem is based on discontinuous numerical fluxes. An invariant region property is proved under the (mild) assumption that the underlying mesh is a \mathbf{B} -triangulation [B. COCKBURN, S. HOU, AND C.-W. SHU, *Math. Comp.*, 54 (1990), pp. 545–581]. This property states that only physically relevant (bounded and non-negative) saturation and concentration values are generated by the scheme. Numerical tests illustrate the accuracy and stability of the proposed method.

Key words. multicomponent viscous flow in porous media, coupled flow-transport problem, discontinuous Galerkin method, invariant region property, polymer flooding, enhanced oil recovery

AMS subject classifications. 65M12, 65M60, 76S05

1. Introduction.

1.1. Scope. We are interested in the numerical simulation of two-phase, multi-component flows in heterogeneous porous media governed by balance laws derived from multi-phase mixture theory. From the diverse applications described by such a general framework (and including for instance, tissue growth or paper manufacturing), here we focus on the process of polymer flooding, which is a mechanism of oil displacement usually employed in enhanced oil recovery (EOR; see [30] and the references therein). In principle, after the so-called secondary oil recovery step (mainly driven by water flooding), a large amount of oil still remains trapped within the rock due to the unfavourable mobility ratio between the water and the displaced oil (see e.g. [13]). Then polymer flooding consists in adding a certain amount of polymers to water to be injected to increase the viscosity of the aqueous phase, and thereby to improve the mobility of the oil and to increase the volumetric sweep efficiency of the flooded reservoir.

Fluid flow in the reservoir is mainly driven by the heterogeneity of the medium and mobility difference between the involved phases. These mechanisms produce a

*This work has been partially funded by the BASAL project CMM, Universidad de Chile and Centro de Investigación en Ingeniería Matemática (CI²MA), Universidad de Concepción; by Fondecyt projects 1170473 and 3150313; by CRHIAM, project CONICYT/FONDAP/15130015; and by the London Mathematical Society.

[†]CI²MA and Departamento de Ingeniería Matemática, Universidad de Concepción, Casilla 160-C, Concepción, Chile. Email: rburger@ing-mat.udec.cl

[‡]CI²MA, Universidad de Concepción, Casilla 160-C, Concepción, Chile. Email: skumar@ci2ma.udec.cl

[§]Mathematical Institute, Oxford University, Andrew Wiles Building, Woodstock Road, OX2 6GG Oxford, UK. E-mail: ruizbaier@maths.ox.ac.uk

[¶]Departamento de Matemáticas, Universidad de La Serena, Av. Cisternas 1200, La Serena, Chile. E-mail: htorres@userena.cl

complex structure arising from the nonlinearities of flow, intrinsic fluid properties, and interaction with transport processes. Thus, any numerical scheme targeted for such applications needs to be accurate enough to describe these components (flow process, high nonlinearities, medium heterogeneities, complex reservoir geometry, high gradients of volume fractions).

We assume that there exist three fluid components: oil, water, and polymers; which flow and interact within two phases: aqueous (wetting, “w”) and oleic (non-wetting, “n”), of respective saturations s_w and s_n such that $s_w + s_n = 1$. The oleic phase consists of oil only, whereas the aqueous phase is conformed by both water and the mixture of \mathcal{M} types of injected polymers of concentrations (mass fractions) $c_1, \dots, c_{\mathcal{M}}$. If we neglect capillary pressure and assume that the fluids are incompressible, immiscible and there are no sources or sinks, then the phasic conservation of mass yields the local continuity equation [7]

$$(1.1) \quad \varphi \frac{\partial s}{\partial t} + \operatorname{div} \mathbf{F} = 0, \quad \mathbf{F} = \mathbf{F}(s, \mathbf{c}, \mathbf{u}, \mathbf{x}), \quad \mathbf{c} := (c_1, \dots, c_{\mathcal{M}})^{\mathsf{T}},$$

where $s := s_w$, t is time, φ is the rock porosity, and the nonlinear flux vector \mathbf{F} depends on s , the concentrations of polymers \mathbf{c} , the volume average flow velocity \mathbf{u} , and spatial position \mathbf{x} . Under the same assumptions, the transport of the polymers in the aqueous phase (cf., e.g., [28, 33]) is described by the continuity equations

$$(1.2) \quad \varphi \frac{\partial}{\partial t}(s c_l) + \frac{\partial}{\partial t}((1 - \varphi) \rho_r a_l(c_l)) + \operatorname{div}(c_l \mathbf{F}) = 0, \quad l = 1, \dots, \mathcal{M},$$

where ρ_r is the density of rock and $a_l(c_l)$ is the adsorption of the polymer c_l per unit mass of the rock. The precise algebraic definition of \mathbf{F} and $a_1, \dots, a_{\mathcal{M}}$ is provided in Section 2.1. Note that the transport equations (1.1) and (1.2) are nonlinearly coupled in s and \mathbf{c} . In addition, the flux function \mathbf{F} usually depends discontinuously on \mathbf{x} since the porous medium is heterogeneous. Finally, the volume average flow velocity \mathbf{u} is determined from the following Brinkman model [5] that represents the momentum and mass conservation of the mixture:

$$(1.3) \quad \begin{aligned} \mathbf{K}(\mathbf{x})^{-1} \mathbf{u} - \operatorname{div}(\mu(s, \mathbf{c}) \boldsymbol{\varepsilon}(\mathbf{u}) - p \mathbf{I}) &= (\rho_w - \rho_n) s \mathbf{g}, \\ \operatorname{div} \mathbf{u} &= j, \end{aligned}$$

where p is the pressure field, $\mathbf{g} = (0, -g)^{\mathsf{T}}$ is the gravitational acceleration, and j is a mass source or sink in the system. Here $\mathbf{K}(\mathbf{x})$ is the absolute permeability tensor of the medium, $\mu(s, \mathbf{c}) \boldsymbol{\varepsilon}(\mathbf{u}) - p \mathbf{I}$ is the Cauchy stress tensor, $\boldsymbol{\varepsilon}(\mathbf{u}) = \frac{1}{2}(\nabla \mathbf{u} + \nabla \mathbf{u}^{\mathsf{T}})$ is the infinitesimal rate of strain and $\mu = \mu(s, \mathbf{c})$ is the viscosity (inverse of the total mobility, defined below) that is assumed uniformly bounded here. The constants ρ_w and ρ_n are the densities of aqueous and oleic phase, respectively. In the case of an isotropic medium, the permeability tensor reduces to $\mathbf{K}(\mathbf{x}) = \kappa(\mathbf{x}) \mathbf{I}$, where $\kappa(\mathbf{x})$ is a scalar function (assumed uniformly bounded), and \mathbf{I} is the identity matrix. Thus, the problem at hand consists in determining the $\mathcal{M} + 5$ scalar components of s , \mathbf{c} , \mathbf{u} and p as functions of \mathbf{x} and t from the coupled system (1.1)–(1.3) of the same numbers of scalar PDEs, supplied with suitable initial and boundary conditions.

Although we neglect capillary pressure and dispersion terms, the predominance of different processes might change the mathematical character of the equations (1.1)–(1.3). In addition, the transport of the polymers is coupled to the phase equations, it changes the phase viscosity, and hence alters flow patterns in the system. To solve (1.1)–(1.3), supplied with suitable boundary conditions, we here adopt a discontinuous

Galerkin (DG) discretisation: a non-conforming Galerkin approximation is introduced for the transport equations (1.1), (1.2) and we utilise a stabilised non-conforming Galerkin method for the flow equations (1.3) based on the treatment by Könnö and Stenberg [23] specifically tailored for Brinkman equations. DG methods feature desirable properties in line with the present application: flexibility for hp -refinement, locking-free approximations, ability to handle discontinuous coefficients, sharp solution interface capturing, and many others (see [37] for its application on a similar transport-flow problem). Moreover, the phenomenon at hand suggests that fluxes may admit discontinuities, and such a feature will be imposed also on the numerical fluxes across element boundaries, following the approach introduced in [34], and here adapted to unstructured simplicial meshes. A Newton method is employed to resolve the main nonlinearity in the transport equations (more precisely, in the isothermal adsorption term). The time discretisation of the transport problems follows a third-order strong stability preserving Runge-Kutta (SSP-RK) method, and the coupling with the flow equations is performed by a sequential iteration scheme. This choice is mainly driven by computational cost and memory requirements (usually much higher in the fully coupled approach).

The main novel contributions in this paper consist in combining high-order space discretisations (which are moreover well suited for parallelisation and useful in large scale EOR simulations) with RK methods, specially targeted for a large class of multicomponent flow problems; and in the analysis of the proposed methods in terms of invariance properties of the discrete saturation and concentration fields.

1.2. Related work. The flow of the fluid components is described by an extension of the two-phase Buckley-Leverett model [7] arising from a fractional flow analysis in [28]. Such a model has been analysed as a hyperbolic system of conservation laws in [17, 18] (see also [19–22, 29, 35]). The additional difficulties due to the nonlinear adsorption terms within the time derivative are addressed in [29, Sect. 1.8] and [34].

Here, that system of mass conservation equations is coupled to a mass and momentum equation for the mixture. In the regime we are interested in, it suffices to incorporate the Stokes-Darcy (or Brinkman) approximation of viscous flow in porous media. Discretisations involving discontinuous elements in combination with finite volume element methods and applied to flow-transport equations in similar contexts can be found in [3, 9–11, 15, 24–26, 31, 32].

1.3. Outline of the paper. We have organised the contents of the paper in the following manner. Section 2 contains an overview of the model problem and the governing equations we will advocate to. The stabilised mixed DG approximation of the flow equations, for a fixed value of the saturation field, is stated in Section 3. Next, the DG scheme for the transport equations is presented in Section 4. We derive the semi-discrete and fully discrete methods, and make precise the choice of discontinuous numerical fluxes. In Section 5 we establish an invariant region property of the transport DG discretisation, and in Section 6 we collect a series of numerical tests illustrating convergence, stability, and performance of the proposed scheme in simplified and more application-oriented cases.

2. Preliminaries.

2.1. Flux vector and adsorption functions. Polymer adsorption determines the success of polymer flooding both technically and economically [14]. This process is modelled here through the terms a_1, \dots, a_M that could be functions of salinity, polymer concentration, and permeability. However, for simplicity, we adopt the simple

Langmuir-type isotherms

$$a_l(c_l) = c_l^{\max} \frac{bc_l}{1 + bc_l}, \quad l = 1, \dots, \mathcal{M},$$

(see [36]), where b is a Langmuir constant and c_l^{\max} is the maximum polymer concentration of the l -th component adsorbed to the rock, which will be specified later.

The nonlinear flux vector $\mathbf{F} = \mathbf{F}(s, \mathbf{c}, \mathbf{u}, \mathbf{x})$ takes the form

$$\mathbf{F}(s, \mathbf{c}, \mathbf{u}, \mathbf{x}) = f(s, \mathbf{c})\mathbf{u} + b(s, \mathbf{c})\mathbf{K}(\mathbf{x})\mathbf{g},$$

where f is the fractional flow function related to aqueous phase given by

$$f(s, \mathbf{c}) = \frac{\lambda_w(s, \mathbf{c})}{\lambda_w(s, \mathbf{c}) + \lambda_n(s)},$$

and $b(s, \mathbf{c}) = f(s, \mathbf{c})\lambda_n(s)(\rho_w - \rho_n)$. The corresponding phase mobilities λ_w and λ_n are expressed in terms of the phase relative permeabilities k_{rw} and k_{rn} and the phase viscosities μ_w and μ_n : $\lambda_w = k_{rw}/\mu_w$ and $\lambda_n = k_{rn}/\mu_n$, and we define $\lambda_{\text{total}} = \lambda_w + \lambda_n$ and $\mu(s, \mathbf{c}) = 1/\lambda_{\text{total}}$. For the relative permeabilities we use the Brooks-Corey model [6], as implemented in [33]. The viscosity μ_n is kept constant as the flow is immiscible and polymers are transported only through the aqueous phase. The viscosity $\mu_w = \mu_w(\mathbf{c})$ depends on the concentration of the polymers and we adopt an expression for μ_w as presented in [33, p. 433], namely $\mu_w(\mathbf{c}) = \mu_w(\mathbf{c}) = \mu_{w,0} + aC$, where C is a scalar variable that can be chosen as $C = c_1 + \dots + c_{\mathcal{M}}$ and a is a positive constant. The original treatment, and our examples, however, are limited to $\mathcal{M} = 1$.

2.2. Initial and boundary conditions. Adequate initial and boundary data complementing (1.1)-(1.3) are necessary to close the system. We will consider the case of a constant initial saturation and concentrations $s_0, c_{l,0}$, a boundary saturation and concentration are assumed on a part of the boundary identified as the inlet, and on the remainder of the boundary we set zero-flux conditions for the saturation and concentrations, together with either Dirichlet conditions for the velocity, or Dirichlet conditions for the pressure field. The presentation of the discretisation will focus on the case of homogeneous Dirichlet velocity and zero-flux saturation and concentration.

3. Mixed non-conforming discretisation for the Brinkman problem. Let us consider a fixed saturation s such that $\mu(s)$ is positive and bounded. We denote standard spaces by $\mathbf{H} := \mathbf{H}^1(\Omega)$, $Q := L_0^2(\Omega)$, multiply (1.3) by suitable test functions $(\mathbf{v}, q) \in \mathbf{H} \times Q$, and integrate the result by parts in such a way that the weak form of (1.3) is as follows: find $(\mathbf{u}, p) \in \mathbf{H} \times Q$ such that

$$(3.1) \quad \mathcal{S}^{s,c}((\mathbf{u}, p), (\mathbf{v}, q)) = \mathcal{F}^s(\mathbf{v}, q) \quad \forall (\mathbf{v}, q) \in \mathbf{H} \times Q,$$

where the involved forms and functionals are defined for all $(\mathbf{u}, p), (\mathbf{v}, q) \in \mathbf{H} \times Q$ as

$$\begin{aligned} \mathcal{S}^{s,c}((\mathbf{u}, p), (\mathbf{v}, q)) &:= a^{s,c}(\mathbf{u}, \mathbf{v}) + b(\mathbf{v}, p) + b(\mathbf{u}, q), \\ \mathcal{F}^s(\mathbf{v}, q) &:= ((\rho_w - \rho_n)s\mathbf{g}, \mathbf{v})_{\Omega} - (j, q)_{\Omega}, \\ a^{s,c}(\mathbf{u}, \mathbf{v}) &:= (\mathbf{K}^{-1}\mathbf{u}, \mathbf{v})_{\Omega} + (\mu(s, \mathbf{c})\boldsymbol{\varepsilon}(\mathbf{u}), \boldsymbol{\varepsilon}(\mathbf{v}))_{\Omega}, \quad b(\mathbf{v}, q) := -(\text{div } \mathbf{v}, q)_{\Omega}. \end{aligned}$$

The discretisation of (1.3) will seek discrete velocities in an $H(\text{div}, \Omega)$ -conforming finite-dimensional space \mathbf{H}_h , associated to a regular partition \mathcal{T}_h of Ω into triangles. We recall that a family of triangulations $\mathcal{F} = \{\mathcal{T}_h\}_{h>0}$ is regular if

$$(3.2) \quad \exists \sigma > 0: \quad h_K/m_K \geq \sigma \quad \forall K \in \mathcal{T}_h, \quad \forall \mathcal{T}_h \in \mathcal{F},$$

where h_K is the diameter of a generic element $K \in \mathcal{T}_h$ and m_K is that of the largest circle inscribed in K . For all $K \in \mathcal{T}_h$ and $e \in \partial K$, we denote by \mathbf{n}_e the normal vector to e outward to K . The set of neighbours of $K \in \mathcal{T}_h$ will be denoted by \mathcal{N}_K . If $L \in \mathcal{N}_K$ is the element sharing with K the edge $e = K|L$, then the normal is denoted component-wise as $\mathbf{n}_e = \mathbf{n}_{K|L} = (n_{K|L}^1, n_{K|L}^2)^\top$.

We here choose Brezzi-Douglas-Marini elements of degree one [4] to approximate \mathbf{u} , and piecewise constant approximations of p , that is

$$\begin{aligned} \mathbf{H}_h &= \{ \mathbf{v} \in H(\operatorname{div}, \Omega) : \mathbf{v}|_K \in \mathbb{P}_1(K)^2 \ \forall K \in \mathcal{T}_h \}, \\ Q_h &= \{ q \in L_0^2(\Omega) : q|_K \in \mathbb{P}_0(K) \ \forall K \in \mathcal{T}_h \}, \end{aligned}$$

which satisfy $\operatorname{div} \mathbf{H}_h \subset Q_h$. As usual, $\mathbb{P}_k(K)$ denotes the space spanned by polynomials of degree less than or equal than k . Since \mathbf{H}_h is not a subspace of \mathbf{H} , additional terms are required in the discrete formulation in order to ensure stability. We adapt to our configuration the interior penalty method introduced in [23], consisting in replacing the bilinear form $a(\cdot, \cdot)$ by its mesh-dependent counterpart

$$\begin{aligned} a_h^s(\mathbf{u}_h, \mathbf{v}_h) &:= (\mathbf{K}^{-1} \mathbf{u}_h, \mathbf{v}_h)_\Omega + \sum_{K \in \mathcal{T}_h} (\mu(s) \boldsymbol{\varepsilon}(\mathbf{u}_h), \boldsymbol{\varepsilon}(\mathbf{v}_h))_K \\ &\quad + \sum_{e \in \mathcal{E}_h} \left(\frac{\alpha}{h_e} \langle \llbracket \mu(s, \mathbf{c}) \mathbf{u}_h \rrbracket, \llbracket \mathbf{v}_h \rrbracket \rangle_e - \langle \llbracket \mu(s, \mathbf{c}) \boldsymbol{\varepsilon}(\mathbf{u}_h) \mathbf{n} \rrbracket, \llbracket \mathbf{v}_h \rrbracket \rangle_e \right. \\ &\quad \left. - \langle \llbracket \mu(s, \mathbf{c}) \boldsymbol{\varepsilon}(\mathbf{v}_h) \mathbf{n} \rrbracket, \llbracket \mathbf{u}_h \rrbracket \rangle_e \right) \end{aligned}$$

for a given stabilisation parameter $\alpha > 0$, where the standard symbols $\llbracket \cdot \rrbracket$ and $\langle \cdot \rangle$ denote the jump and mean values, respectively, of a quantity across a point on e . The non-conforming method associated to (3.1) can now be formulated as follows: for fixed saturation s and polymer concentration \mathbf{c} , find $(\mathbf{u}_h, p_h) \in \mathbf{H}_h \times Q_h$ such that

$$(3.3) \quad \mathcal{S}_h^{s, \mathbf{c}}((\mathbf{u}_h, p_h), (\mathbf{v}_h, q_h)) = \mathcal{F}^s(\mathbf{v}_h, q_h) \quad \forall (\mathbf{v}_h, q_h) \in \mathbf{H}_h \times Q_h,$$

where we define

$$\mathcal{S}_h^{s, \mathbf{c}}((\mathbf{u}_h, p_h), (\mathbf{v}_h, q_h)) := a_h^{s, \mathbf{c}}(\mathbf{u}_h, \mathbf{v}_h) + b(\mathbf{v}_h, p_h) + b(\mathbf{u}_h, q_h).$$

The solvability, consistency, and stability of this formulation, along with a priori and a posteriori error bounds for (3.3), have been derived in [23]. The suggested energy norms depend on the meshsize h and, as in [23], also on the permeability and viscosity:

$$(3.4) \quad \begin{aligned} \|\mathbf{v}\|_h^2 &:= \|\mathbf{v}\|_{0, \Omega}^2 + \eta \left(\sum_{K \in \mathcal{T}_h} \|\boldsymbol{\varepsilon}(\mathbf{v})\|_{0, K}^2 + \sum_{e \in \mathcal{E}_h} \frac{1}{h_e} \|\llbracket \mathbf{v} \cdot \boldsymbol{\tau} \rrbracket\|_{0, e}^2 \right), \\ \|q\|_h^2 &:= \|q\|_{0, \Omega}^2 + \sum_{e \in \mathcal{E}_h} \frac{h_e}{h_e^2 + \eta} \|\llbracket q \rrbracket\|_{0, e}^2, \quad \text{where } \eta = \kappa_{\max} \mu_{\max}. \end{aligned}$$

4. A DG method for the transport equations.

4.1. General formulation and semi-discrete approximation. We multiply the transport equations (1.1) and (1.2) by $\phi_s, \phi_{c_l} \in V := H^1(\Omega)$, respectively, where $l = 1, \dots, \mathcal{M}$, and integrate the results by parts over an arbitrary subset $R \subset \Omega$ to

obtain the following local weak formulation, where $F(s, \mathbf{c}, \mathbf{u}) := F(s, \mathbf{c}, \mathbf{u}, \cdot)$:

$$(4.1) \quad \begin{aligned} & \frac{d}{dt}(\varphi s, \phi_s)_R - (\mathbf{F}(s, \mathbf{c}, \mathbf{u}), \nabla \phi_s)_R + \langle \mathbf{F}(s, \mathbf{c}, \mathbf{u}) \cdot \mathbf{n}_R, \phi_s \rangle_{\partial R} = 0, \\ & \frac{d}{dt}(\varphi s c_l + (1 - \varphi) \rho_r a_l(c_l), \phi_{c_l})_R - (c_l \mathbf{F}(s, \mathbf{c}, \mathbf{u}), \nabla \phi_{c_l})_R \\ & \quad + \langle c_l \mathbf{F}(s, \mathbf{c}, \mathbf{u}) \cdot \mathbf{n}_R, \phi_{c_l} \rangle_{\partial R} = 0, \quad l = 1, \dots, \mathcal{M}, \end{aligned}$$

where \mathbf{n}_R denotes the outward unit normal to ∂R . Next, we introduce the following finite element space (non-conforming to V) for $k > 0$:

$$V_h := \{ \phi \in L^2(\Omega) : \phi|_K \in \mathbb{P}_k(K) \ \forall K \in \mathcal{T}_h \},$$

and consider its localisation to the element K , $V_h(K)$, so that a semi-discrete DG method for (4.1) reads: for $0 < t \leq T$, and for a fixed discrete velocity \mathbf{u}_h , find $(s_h(t), \mathbf{c}_h(t)) \in V_h \times V_h^{\mathcal{M}}$ such that for a given $K \in \mathcal{T}_h$,

$$(4.2) \quad \begin{aligned} & \frac{d}{dt}(\varphi s_h, \phi_s)_K - (\mathbf{F}(s_h, \mathbf{c}_h, \mathbf{u}_h), \nabla \phi_s)_K + \langle \hat{F}, \phi_s \rangle_{\partial K} = 0 \quad \forall \phi_s \in V_h(K), \\ & \frac{d}{dt}(\varphi s_h c_{lh} + (1 - \varphi) \rho_r a_l(c_{lh}), \phi_{c_l})_K - (c_{lh} \mathbf{F}(s_h, \mathbf{c}_h, \mathbf{u}_h), \nabla \phi_{c_l})_K \\ (4.3) \quad & \quad + \langle \hat{G}_l, \phi_{c_l} \rangle_{\partial K} = 0 \quad \forall \phi_{c_l} \in V_h(K), \quad l = 1, \dots, \mathcal{M}, \end{aligned}$$

where \hat{F} and $\hat{G}_1, \dots, \hat{G}_{\mathcal{M}}$ are numerical fluxes specified in the next section.

4.2. Choice of numerical fluxes. In this section (and whenever clear from the context) the explicit dependence on the time variable will be dropped. As in [12], we consider the flux approximation

$$\mathbf{F}(s_h, \mathbf{c}_h, \mathbf{u}_h, \mathbf{x}^K) \cdot \mathbf{n}_e \approx \hat{F}(s_h(\tilde{\mathbf{x}}^K), s_h(\hat{\mathbf{x}}^K), \mathbf{c}_h(\tilde{\mathbf{x}}^K), \mathbf{c}_h(\hat{\mathbf{x}}^K), \mathbf{u}_h, \mathbf{n}_e),$$

where $\phi_h(\tilde{\mathbf{x}}^K)$ and $\phi_h(\hat{\mathbf{x}}^K)$ represent the traces of the approximate generic field ϕ (e.g. concentration and saturation) taken from the interior and exterior of K , respectively. In addition, the numerical fluxes $\hat{G}_1, \dots, \hat{G}_{\mathcal{M}}$ in (4.3) are defined as follows:

$$(4.4) \quad \hat{G}_l = \begin{cases} c_{lh}(\tilde{\mathbf{x}}^K) \hat{F} & \text{if } \hat{F} > 0, \\ c_{lh}(\hat{\mathbf{x}}^K) \hat{F} & \text{otherwise,} \end{cases} \quad l = 1, \dots, \mathcal{M},$$

depending on the characteristic speed of the local polymer concentrations c_{lh} (see [34, § 2]). Note that it suffices to define \hat{F} to make precise the definitions in (4.4), and here we employ discontinuous fluxes as proposed in [34], together with the numerical flux formulation of [8, §3.4]. There, one treats $\mathbf{c}(\mathbf{x})$ as a discontinuous datum across the boundaries. That is, on each $e \subset \partial K$ we consider

$$(4.5) \quad \hat{F}(\alpha, \beta, \mathbf{c}_h(\tilde{\mathbf{x}}^K, t), \mathbf{c}_h(\hat{\mathbf{x}}^K, t), \mathbf{u}_h, \mathbf{n}_e) = \hat{F}_1(\alpha, \beta, n_e^1) + \hat{F}_2(\alpha, \beta, n_e^2),$$

where the components \hat{F}_1 and \hat{F}_2 are the DFLU numerical fluxes [1] computed as

$$\begin{aligned} F_{e,i}^-(\cdot) &:= F_i(\cdot, \mathbf{c}_h(\tilde{\mathbf{x}}^K), \mathbf{u}_h(\mathbf{x}), \mathbf{x}^-) n_e^i, \\ F_{e,i}^+(\cdot) &:= F_i(\cdot, \mathbf{c}_h(\hat{\mathbf{x}}^K), \mathbf{u}_h(\mathbf{x}), \mathbf{x}^+) n_e^i, \quad i = 1, 2, \\ a \vee b &:= \max\{a, b\}, \quad a \wedge b := \min\{a, b\} \quad \text{for all } a, b \in \mathbb{R}. \end{aligned}$$

Since the components $F_{e,i}^\pm$ satisfy the hypotheses (H_1) and (H_2) of [1], we get

$$(4.6) \quad \hat{F}_i(\alpha, \beta, n^i) = \operatorname{sgn}(n^i) [\operatorname{sgn}(n^i) F_{e,i}^- (\operatorname{sgn}(n^i) \delta_i^1) \vee \operatorname{sgn}(n^i) F_{e,i}^+ (\operatorname{sgn}(n^i) \delta_i^2)],$$

where we have replaced n_e^i and $F_{e,i}^\pm$ by n^i and F_i^\pm and set for $i = 1, 2$

$$\begin{aligned} \delta_i^1 &:= \operatorname{sgn}(n^i) \alpha \vee \operatorname{sgn}(n^i) \theta_{F_i^-}, & \delta_i^2 &:= \operatorname{sgn}(n^i) \beta \wedge \operatorname{sgn}(n^i) \theta_{F_i^+}, \\ \text{and } \theta_{F_i^\pm} &\text{ are chosen such that } F_i^\pm(\theta_{F_i^\pm}) = \min_{0 \leq \phi \leq 1} (\operatorname{sgn}(n^i) F_i^\pm(\phi)). \end{aligned}$$

LEMMA 4.1. *For fixed values of $\mathbf{u}_h(\mathbf{x})$, $\mathbf{c}_h(\check{\mathbf{x}}^K)$, and $\mathbf{c}_h(\hat{\mathbf{x}}^K)$, the numerical flux \hat{F} defined by (4.5) is monotone (i.e., it is a non-decreasing function of α and a non-increasing function of β) and conservative, that is*

$$\hat{F}(\alpha, \beta, \mathbf{c}_h(\check{\mathbf{x}}^K), \mathbf{c}_h(\hat{\mathbf{x}}^K), \mathbf{u}_h, \mathbf{n}) = -\hat{F}(\beta, \alpha, \mathbf{c}_h(\check{\mathbf{x}}^K), \mathbf{c}_h(\hat{\mathbf{x}}^K), \mathbf{u}_h, -\mathbf{n}).$$

The proof of Lemma 4.1 follows along the lines of [8]. We note that the numerical fluxes \hat{F} and $\hat{G}_1, \dots, \hat{G}_M$ are not consistent in the usual sense as the corresponding flux functions are discontinuous in \mathbf{x} . However, this does not compromise the possibility of deriving convergence of the scheme, because the stability still holds (see [2, p. 181]).

4.3. Fully-discrete scheme for the transport equations. We insert the corresponding numerical fluxes \hat{F} and \hat{G}_l into the expressions (4.2) and (4.3) and approximate the boundary and interior integrals by suitable quadrature formulas over each edge e of an element K . Specifically, for ease of notation we denote for a given element K and interior node \mathbf{x}_i^K , $i = 1, \dots, p$, the argument of \mathbf{F} by

$$\mathbf{y}_{K,i,h}(t) := (s_h(\mathbf{x}_i^K, t), \mathbf{c}_h(\mathbf{x}_i^K, t), \mathbf{u}_h(\mathbf{x}_i^K), \mathbf{x}_i^K),$$

and for each element K , edge $e = K|L \in \partial K$ and boundary node \mathbf{x}_i^e , $i = 1, \dots, q$, the argument of \hat{F} and \hat{G}_l , $l = 1, \dots, M$, by

$$\mathbf{w}_{e,i,h}(t) := (s_h(\check{\mathbf{x}}_i^e, t), s_h(\hat{\mathbf{x}}_i^e, t), \mathbf{c}_h(\check{\mathbf{x}}_i^e, t), \mathbf{c}_h(\hat{\mathbf{x}}_i^e, t), \mathbf{u}_h^e, \mathbf{x}_i^e, \mathbf{n}_e).$$

Then (4.2) and (4.3) are approximated as follows, where without loss of generality we choose $\phi_h = \phi_s = \phi_{c_l}$:

$$(4.7) \quad \begin{aligned} & \frac{d}{dt} (\varphi s_h(\mathbf{x}, t), \phi_h(\mathbf{x}))_K - \sum_{i=1}^p \bar{\omega}_i \mathbf{F}(\mathbf{y}_{K,i,h}(t)) \cdot \nabla \phi_h(\mathbf{x}_i^K) |K| \\ & + \sum_{e \in \partial K} \sum_{i=1}^q \omega_i \hat{F}(\mathbf{w}_{e,i,h}(t)) \phi_h(\mathbf{x}_i^e) |e| = 0, \\ & \frac{d}{dt} (\pi_h^l, \phi_h(\mathbf{x}))_K - \sum_{i=1}^p \bar{\omega}_i c_{lh}(\mathbf{x}_i^K, t) \mathbf{F}(\mathbf{y}_{K,i,h}(t)) \cdot \nabla \phi_h(\mathbf{x}_i^K) |K| \\ & + \sum_{e \in \partial K} \sum_{i=1}^q \omega_i \hat{G}_l(\mathbf{w}_{e,i,h}(t)) \phi_h(\mathbf{x}_i^e) |e| = 0, \quad l = 1, \dots, M, \end{aligned}$$

where $\pi_h^l := \varphi s_h c_{lh} + (1 - \varphi) \rho_r a_l(c_{lh})$ and $\bar{\omega}_i$ and ω_i are the weights corresponding to the interior and boundary quadrature points \mathbf{x}_i^K and \mathbf{x}_i^e , respectively. We choose

a basis $\{\psi_1, \dots, \psi_J\}$ for the space $\mathbb{P}_k(K)$ and write the approximate variables as

$$s_h(\mathbf{x}, t) \approx \sum_{j=1}^J s_j^K(t) \psi_j(\mathbf{x}), \quad \pi_h^l(\mathbf{x}, t) \approx \sum_{j=1}^J \pi_j^{l,K}(t) \psi_j(\mathbf{x}), \quad \forall \mathbf{x} \in K, \quad l = 1, \dots, \mathcal{M}.$$

Choosing $\phi_h = \psi_j$, $j = 1, \dots, J$, we can recast (4.7) as the ODE system

$$(4.8) \quad \frac{d}{dt} \varphi \mathbf{s}_h^K(t) = -\mathbf{A}^{-1}(\mathbf{w} + \mathbf{z}); \quad \frac{d}{dt} \boldsymbol{\pi}_h^{l,K}(t) = -\mathbf{A}^{-1}(\hat{\mathbf{w}}_l + \hat{\mathbf{z}}_l), \quad l = 1, \dots, \mathcal{M},$$

where $\mathbf{s}_h^K(t) := (s_1^K(t), \dots, s_J^K(t))^T$ and $\boldsymbol{\pi}_h^{l,K}(t) := (\pi_1^{l,K}(t), \dots, \pi_J^{l,K}(t))^T$. The entries of the matrix $\mathbf{A} = (a_{jk})_{J \times J}$ and the vectors \mathbf{w} , \mathbf{z} , $\hat{\mathbf{z}}$, and $\hat{\mathbf{w}}_l$ are given by

$$\begin{aligned} a_{jk} &= (\psi_j, \psi_k)_K, \quad w_k = -\sum_{i=1}^p \bar{\omega}_i \mathbf{F}(\mathbf{y}_{K,i,h}(t)) \cdot \nabla \psi_k(\mathbf{x}_i^K) |K|, \\ z_k &= \sum_{e \in \partial K} \sum_{i=1}^q \omega_i \hat{F}(\mathbf{w}_{e,i,h}(t)) \psi_k(\mathbf{x}_i^e) |e|, \quad \hat{z}_k = \sum_{e \in \partial K} \sum_{i=1}^q \omega_i \hat{G}(\mathbf{w}_{e,i,h}(t)) \psi_k(\mathbf{x}_i^e) |e|, \\ \hat{w}_{l,k} &= -\sum_{i=1}^p \bar{\omega}_i c_{lh}(\mathbf{x}_i^K, t) \mathbf{F}(\mathbf{y}_{K,i,h}(t)) \cdot \nabla \psi_k(\mathbf{x}_i^K) |K|. \end{aligned}$$

The semi-discrete system (4.8) is evolved in time with a third order SSP-RK method [27]. The key point in here is not to split the numerical flux during the SSP-RK stages. Usually the needed fluxes are obtained by solution of local Riemann problems for (1.1) and (1.2), or by approximation via a Lax-Friedrichs method. However, the former strategy can be quite expensive in most cases and the latter might be highly inefficient in capturing shocks. Then, following [34] we can derive discontinuous numerical fluxes for the coupled equations (4.8) by decoupling the system into scalar equations. This is achieved by treating the approximate polymer concentration as a discontinuous coefficient entering the numerical flux (cf. [34, §2.4]). The procedure is illustrated for a forward Euler scheme by writing the set of equations

$$\begin{aligned} \varphi \mathbf{s}_h^K(t^{n+1}) &= \varphi \mathbf{s}_h^K(t^n) - \mathbf{A}^{-1}(\mathbf{w} + \mathbf{z}), \\ \boldsymbol{\pi}_h^{l,K}(t^{n+1}) &= \boldsymbol{\pi}_h^{l,K}(t^n) - \mathbf{A}^{-1}(\hat{\mathbf{w}}_l + \hat{\mathbf{z}}_l), \quad l = 1, \dots, \mathcal{M}, \end{aligned}$$

which in turn amounts to determine the value of \hat{F} in the vectors \mathbf{z}_k and $\hat{\mathbf{z}}_k$, from the expression (4.5), where the arguments are the known concentrations, saturation and velocity at time t^n . Thereby the values $s_h^K(t^{n+1})$ and $\pi_h^{l,K}(t^{n+1})$ are computed separately, and the approximate solutions at time t^{n+1} are updated by

$$\begin{aligned} s_h(\mathbf{x}, t^{n+1}) &= (\psi_1(\mathbf{x}), \psi_2(\mathbf{x}), \dots, \psi_L(\mathbf{x})) \mathbf{s}_h^K(t^{n+1}) \quad \forall \mathbf{x} \in K, \\ \pi_h^l(\mathbf{x}, t^{n+1}) &= (\psi_1(\mathbf{x}), \psi_2(\mathbf{x}), \dots, \psi_L(\mathbf{x})) \boldsymbol{\pi}_h^{l,K}(t^{n+1}) \quad \forall \mathbf{x} \in K, \quad l = 1, \dots, \mathcal{M}. \end{aligned}$$

Then the approximate concentrations c_{lh}^{n+1} are recovered by a Newton method solving

$$\pi_h^l(\mathbf{x}, t^{n+1}) = \varphi s_h^{n+1} c_{lh}^{n+1} + (1 - \varphi) \rho_r a_l (c_{lh}^{n+1}).$$

5. Invariant region for the discrete transport equations. In this section we assess the L^∞ stability of the DG discretisation applied to the coupled system (1.1), (1.2). We will show that the element averages of the DG solutions

$$\bar{s}_K^n := \frac{1}{|K|} \int_K s_h(\mathbf{x}, t^n) d\mathbf{x}, \quad \bar{c}_{lK}^n := \frac{1}{|K|} \int_K c_{lh}(\mathbf{x}, t^n) d\mathbf{x}, \quad l = 1, \dots, \mathcal{M},$$

satisfy a maximum principle. We recall that in each K the approximate solutions $s_h(\mathbf{x}, t^n)$ and $c_{lh}(\mathbf{x}, t^n)$ are polynomials, here denoted by $p_{s,K}^n$ and $p_{c_l,K}^n$, respectively. As the SSP-RK scheme preserves the stability of the forward Euler method for the same timestep restriction (see [16, 27]), it suffices to analyse the latter case.

5.1. Invariant region for the discrete saturation. Taking $\phi_h \equiv 1$ and discretising (4.7) in time with a forward Euler scheme leads to

$$(5.1) \quad \begin{aligned} \bar{s}_K^{n+1} &= \bar{s}_K^n - \frac{\Delta t}{\varphi|K|} \sum_{e \in \partial K} \sum_{i=1}^q \omega_i \hat{F}_{e,i}|e|, \\ \bar{s}_K^{n+1} \bar{c}_{lK}^{n+1} + \frac{1-\varphi}{\varphi} \rho_r a_l(\bar{c}_{lK}^{n+1}) &= \bar{s}_K^n \bar{c}_{lK}^n + \frac{1-\varphi}{\varphi} \rho_r a_l(\bar{c}_{lK}^n) - \frac{\Delta t}{\varphi|K|} \sum_{e \in \partial K} \sum_{i=1}^q \omega_i \hat{G}_{e,i}|e|, \end{aligned}$$

where we use the convention

$$\hat{F}_{e,i} := \hat{F}(\mathbf{w}_{e,i,h}(t)); \quad \hat{G}_{e,i} := \hat{G}_l(\mathbf{w}_{e,i,h}(t)), \quad l = 1, \dots, \mathcal{M}.$$

We need to compute the edge integral in (4.7) exactly, for polynomials of degree $2k+1$ (see [12, Prop. 2.1]). We choose a $(k+1)$ -point Gauss rule, where the $q = k+1$ quadrature points corresponding to each edge $e \in \partial K$ are $\{\mathbf{x}_i^e, i = 1, \dots, q\}$.

In order to verify the maximum principle for the discrete saturation resulting from (5.1), one can proceed along the lines of [8]. The key step consists in writing the approximate value as a function of $6q + p$ scalar arguments as follows:

$$(5.2) \quad \bar{s}_K^{n+1} = H(s_h(\tilde{\mathbf{x}}_i^e, t^n), s_h(\hat{\mathbf{x}}_i^e, t^n) : i = 1, \dots, q, e \in \partial K; s_h(\mathbf{x}_j^K, t^n) : j = 1, \dots, p).$$

Expression (5.2) can be obtained once we formulate the approximate average in terms of the DG solution computed at the quadrature points. Then the concentration can be regarded as a discontinuous coefficient in the numerical flux, so that the following result can readily be proved (repeating the arguments in the proof of [8, Lemma 4.1]).

LEMMA 5.1. *The function H in (5.2) is increasing in each of its arguments provided the following CFL condition is satisfied, where $\hat{\omega}_1$ is the first weight of the Gauss-Lobatto quadrature rule on $[-1/2, 1/2]$:*

$$(5.3) \quad \frac{\Delta t}{\varphi|K|} \sum_{e \in \partial K} |e| \leq \frac{2}{3} \hat{\omega}_1.$$

In turn, we can assert the following result.

THEOREM 5.1. *The DG solution computed from (4.2), using the DFLU numerical flux (4.5)–(4.6) and a forward Euler time stepping, satisfies $0 \leq \bar{s}_K^{n+1} \leq 1$ for all $n \geq 0$, provided condition (5.3) is met and $p_{s,K}^n(\mathbf{x}) \in [0, 1]$, where $p_{s,K}^n$ is the computed DG polynomial at the time step t^n .*

We remark that at time t^n , the cell-wise DG polynomial $p_{s,K}^n$ need not assume values in $[0, 1]$. Actually, a *linear* scaling limiter (cf. [8, p. 140]) is applied at this stage to enforce this condition, but a bound on the evolved DG solution is not guaranteed.

5.2. Invariant region for the element-wise concentration. In order to verify whether the computed concentrations lie within the bound of initial concentrations, we first consider a splitting of the numerical fluxes as

$$\begin{aligned}\hat{F}_{e,i} &= \hat{F}_{e,i}^+ + \hat{F}_{e,i}^-, \quad \text{where } \hat{F}_{e,i}^+ = \max\{0, \hat{F}_{e,i}\} \text{ and } \hat{F}_{e,i}^- = \min\{0, \hat{F}_{e,i}\}, \\ \hat{G}_{e,i} &= \check{c}_{e,i} \hat{F}_{e,i}^+ + \hat{c}_{e,i} \hat{F}_{e,i}^-, \quad \text{where } \check{c}_{e,i} = c_h(\hat{\mathbf{x}}_i^e, t), \hat{c}_{e,i} = c_h(\hat{\mathbf{x}}_i^e, t),\end{aligned}$$

where, if no confusion arises, we suppress the index l of the concentration and adsorption terms for the rest of this section. In analogy to the analysis for the discrete saturation, here we choose $\phi_h \equiv 1$ in the second equation of (4.7) and apply a forward Euler scheme giving

$$\begin{aligned}(5.4) \quad & \bar{s}_K^{n+1} \bar{c}_K^{n+1} + \frac{1-\varphi}{\varphi} \rho_r a(\bar{c}_K^{n+1}) \\ &= \bar{s}_K^n \bar{c}_K^n + \frac{1-\varphi}{\varphi} \rho_r a(\bar{c}_K^n) - \frac{\Delta t}{\varphi |K|} \sum_{e \in \partial K} \sum_{i=1}^q |e| \omega_i (\check{c}_{e,i} \hat{F}_{e,i}^+ + \hat{c}_{e,i} \hat{F}_{e,i}^-).\end{aligned}$$

For a given edge $e = K|L$ and each quadrature point \mathbf{x}_i^e we can expand the DG solution as

$$(5.5) \quad c_h(\check{\mathbf{x}}_i^e, t^n) = \bar{c}_K^n + \tilde{c}_{K,L,i}^n \quad \text{and} \quad c_h(\hat{\mathbf{x}}_i^e, t^n) = \bar{c}_L^n + \tilde{c}_{L,K,i}^n$$

(using both interior and exterior points), where the terms with tildes indicate a given fluctuation around the elementary averages. Next we denote by $\mathbf{c}_{e,i}^b = c^b(\mathbf{x}_i^e)$ the vector of predetermined boundary values of the concentration.

The following geometric property is essential for the derivation of the local maximum principle.

LEMMA 5.2. *Any smooth function $\phi : \mathbb{R}^2 \rightarrow \mathbb{R}$ can be expressed as $\bar{\phi}_K = \phi(\mathbf{x}_K) + \mathcal{O}(h_K^2)$, where \mathbf{x}_K is the barycentre of $K \in \mathcal{T}_h$.*

Proof. As \mathbf{x}_K is the barycentre of K , we can write $\mathbf{x}_K = \frac{1}{|K|} \int_K \boldsymbol{\xi} \, d\boldsymbol{\xi}$. Moreover, setting $\nabla \phi(\mathbf{x}_K) := \nabla \phi|_{\mathbf{x}_K}$, we can assert that

$$\begin{aligned}\int_K (\mathbf{x} - \mathbf{x}_K) \cdot \nabla \phi(\mathbf{x}_K) \, d\mathbf{x} &= \int_K \left(\mathbf{x} - \frac{1}{|K|} \int_K \boldsymbol{\xi} \, d\boldsymbol{\xi} \right) \cdot \nabla \phi(\mathbf{x}_K) \, d\mathbf{x} \\ &= \int_K \mathbf{x} \cdot \nabla \phi(\mathbf{x}_K) \, d\mathbf{x} - \int_K \boldsymbol{\xi} \cdot \nabla \phi(\mathbf{x}_K) \, d\boldsymbol{\xi} \left(\frac{1}{|K|} \int_K 1 \, d\mathbf{x} \right) \\ &= \int_K \mathbf{x} \cdot \nabla \phi(\mathbf{x}_K) \, d\mathbf{x} - \int_K \boldsymbol{\xi} \cdot \nabla \phi(\mathbf{x}_K) \, d\boldsymbol{\xi} = 0.\end{aligned}$$

Utilising the Taylor expansion $\phi(\mathbf{x}) = \phi(\mathbf{x}_K) + (\mathbf{x} - \mathbf{x}_K) \cdot \nabla \phi(\mathbf{x}_K) + \mathcal{O}(h_K^2)$ now yields

$$\begin{aligned}\bar{\phi} &:= \frac{1}{|K|} \int_K \phi(\mathbf{x}) \, d\mathbf{x} = \frac{1}{|K|} \int_K (\phi(\mathbf{x}_K) + (\mathbf{x} - \mathbf{x}_K) \cdot \nabla \phi(\mathbf{x}_K) + \mathcal{O}(h_K^2)) \, d\mathbf{x} \\ &= \phi(\mathbf{x}_K) + \frac{1}{|K|} \int_K (\mathbf{x} - \mathbf{x}_K) \cdot \nabla \phi(\mathbf{x}_K) \, d\mathbf{x} + \frac{1}{|K|} \int_K \mathcal{O}(h_K^2) \, d\mathbf{x} \\ &= \phi(\mathbf{x}_K) + \frac{1}{|K|} \int_K \mathcal{O}(h_K^2) \, d\mathbf{x} = \phi(\mathbf{x}_K) + \mathcal{O}(h_K^2).\end{aligned}$$

This completes the proof. \square

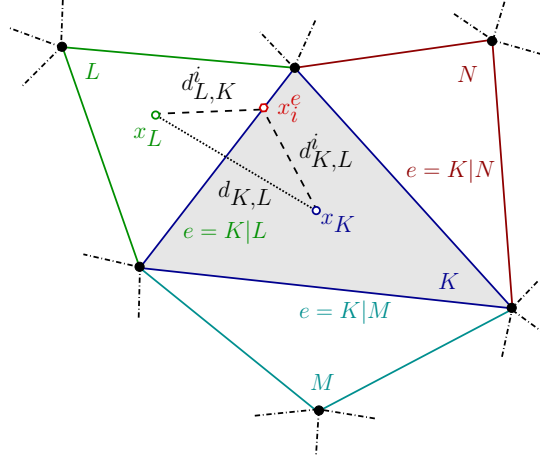


FIG. 1. Sketch of a given element K and its neighbours L, M, N , in a \mathbf{B} -triangulation.

In addition, we require the concept of \mathbf{B} -triangulations [12], defined in what follows, where for sake of simplicity, for any edge lying on $\partial\Omega$ its adjacent element will be treated as a ghost cell.

Let \mathbf{x}_K and \mathbf{x}_L denote the barycentre of K and L , respectively; and \mathbf{x}_e denote the midpoint of the edge e (see Figure 1). For $K \in \mathcal{T}_h$ we denote

$$(5.6) \quad d_{K,L} := \begin{cases} \mathbf{x}_e - \mathbf{x}_K & \text{if } L \text{ is a ghost cell,} \\ \mathbf{x}_L - \mathbf{x}_K & \text{otherwise.} \end{cases}$$

We identify the segments $d_{K,L}^i = \mathbf{x}_i^e - \mathbf{x}_K$, for all $e = K|L$, and recall the following definitions from [12].

DEFINITION 5.1. A mesh \mathcal{T}_h is a \mathbf{B} -triangulation if for any $K \in \mathcal{T}_h$ and pairs $d_{K,L}^i, d_{L,K}^i$, with $i = 1, \dots, q$ indicating an index for the quadrature points, one can choose segments $d_{K,M}$ and $d_{K,N}$ (defined in (5.6) where $M, N \in \mathcal{N}_K$) such that

$$-d_{K,L}^i = \theta_{K,L,M}^i d_{K,M} + \theta_{K,L,N}^i d_{K,N}, \quad d_{L,K}^i = \vartheta_{L,K,M}^i d_{K,M} + \vartheta_{L,K,N}^i d_{K,N},$$

for some non-negative constants $\theta_{K,L,M}^i, \theta_{K,L,N}^i, \vartheta_{L,K,M}^i$ and $\vartheta_{L,K,N}^i$.

DEFINITION 5.2. A family of triangulations $\{\mathcal{T}_h\}_{h>0}$ is \mathbf{B} -uniform if each triangulation \mathcal{T}_h is a \mathbf{B} -triangulation, and if there exists a constant $\nu > 0$ such that

$$\forall K \in \mathcal{T}_h, h > 0 : \forall L, M, N \in \mathcal{N}_K : \forall i = 1, \dots, q : \\ \theta_{K,L,M}^i, \theta_{K,L,N}^i, \vartheta_{L,K,M}^i, \vartheta_{L,K,N}^i \in [0, \nu].$$

The constant ν depends on the choice of $\{\mathcal{T}_h\}_{h>0}$. For acute angle triangles, the existence of such a ν can be verified and the following result holds (see [12]).

LEMMA 5.3. If \mathcal{F} is a family of meshes consisting of acute triangles, then it is \mathbf{B} -uniform with constant $\nu = 2\sigma^3(1 + \sigma^2)^{3/2}$, where σ is as in (3.2).

Going back to our numerical scheme we present a useful result (provided in [12, (2.14)] without proof), and we postpone the proof to the Appendix.

LEMMA 5.4. *If c_h is a smooth function (inside K), then*

$$(5.7) \quad -\bar{c}_{K,L,i}^n = \theta_{K,L,M}^i \Delta_{K,M} + \theta_{K,L,N}^i \Delta_{K,N} + \mathcal{O}(h^2),$$

$$(5.8) \quad \bar{c}_{L,K,i}^n = \vartheta_{L,K,M}^i \Delta_{K,M} + \vartheta_{L,K,N}^i \Delta_{K,N} + \mathcal{O}(h^2),$$

where we define

$$\Delta_{K,L} = \begin{cases} \bar{c}_L^n - \bar{c}_K^n & \text{if } e = K|L \in \partial K, \\ \bar{c}_e^b - \bar{c}_K^n & \text{if } e \in \partial K \cap \partial\Omega, \end{cases} \quad \text{where } \bar{c}_e^b := \frac{1}{|e|} \int_e c^b \, ds,$$

and $\theta_{K,L,M}^i$, $\theta_{K,L,N}^i$, $\vartheta_{L,K,M}^i$ and $\vartheta_{L,K,N}^i$ are as in Definition 5.1.

Lemma 5.4 indicates that for a suitable choice of $\kappa \geq 1$ we can ensure that

$$(5.9) \quad \bar{c}_{K,L,i}^n \in I(0, \kappa \mathcal{C}_{K,L,i}), \quad \bar{c}_{L,K,i}^n \in I(0, \kappa \mathcal{C}_{L,K,i}),$$

where

$$\begin{aligned} \mathcal{C}_{K,L,i} &= -(\theta_{K,L,M}^i \Delta_{K,M} + \theta_{K,L,N}^i \Delta_{K,N}), \\ \mathcal{C}_{L,K,i} &= \vartheta_{L,K,M}^i \Delta_{K,M} + \vartheta_{L,K,N}^i \Delta_{K,N}, \end{aligned}$$

and where for finitely many numbers a_1, \dots, a_J , the interval I is

$$I(a_1, \dots, a_J) := [\min\{a_1, \dots, a_J\}, \max\{a_1, \dots, a_J\}].$$

Note that in the regions where c_h is smooth, conditions (5.9) are satisfied as a consequence of Lemma 5.4. However, if the solution is discontinuous then we require a projection operator $\mathbb{A}\Pi_h$ (defined in [12] for the class of \mathbf{B} -triangulations), which in particular, does not compromise the initial order of accuracy.

DEFINITION 5.3 (cf. [12]). *The quantity $\mathbb{A}\Pi_h(c_h)|_K$ is defined as the projection by $\mathbb{A}\Pi_h : \mathbb{V}_h \rightarrow \mathbb{V}_h$ of $c_h|_K$ into the non-empty convex set*

$$Q(K, c_h) := \{\varphi : \Omega \rightarrow \mathbb{R} \mid \varphi|_K \in \mathbb{P}_k(K), \bar{\varphi} = \bar{c}_h, \text{ and (5.9) holds}\}.$$

LEMMA 5.5. *If c_h is computed on a \mathbf{B} -uniform family, then*

$$\begin{aligned} -\bar{c}_{K,L,i}^n &= \theta_{K,L,M}^i \Delta_{K,M} + \theta_{K,L,N}^i \Delta_{K,N}, \\ \bar{c}_{L,K,i}^n &= \vartheta_{L,K,M}^i \Delta_{K,M} + \vartheta_{L,K,N}^i \Delta_{K,N}, \end{aligned}$$

where $\Delta_{K,M}$, $\Delta_{K,N}$ and the constants θ^i and ϑ^i are as in Definition 5.1.

Proof. The proof follows from a direct application of Lemma 5.4 (including conditions (5.9)) together with the projection operator. \square

We are now in position to state the local maximum principle for c_h .

THEOREM 5.2. *Let c_h be the discrete concentration resulting from (4.7), advanced in time using the forward Euler scheme on a \mathbf{B} -uniform triangulation together with the projection in Definition 5.3. Then*

$$(5.10) \quad \bar{c}_K^{n+1} \in I(\bar{c}_K^n; \bar{c}_L^n : L \in \mathcal{N}_K; \bar{c}_e^b, c_{1,e}^b, \dots, c_{q,e}^b : e \in \partial K \cap \partial\Omega) \quad \forall K \in \mathcal{T}_h,$$

provided that $\omega_i \geq 0$ for all i , and

$$(5.11) \quad \text{cfl} := \Delta t \sup_{e \in \partial K : K \in \mathcal{T}_h} \frac{|e|}{\varphi|_K} S \leq \frac{1}{5 + 40\kappa\nu},$$

where

$$S = \sup_{s \in [0,1]} \left\{ \frac{\partial F_1}{\partial s}, \frac{\partial F_2}{\partial s}, F_1 \left(s + \frac{1-\varphi}{\varphi} \rho_r a' \right)^{-1}, F_2 \left(s + \frac{1-\varphi}{\varphi} \rho_r a' \right)^{-1} \right\}.$$

Proof. Adding and subtracting $\bar{s}_K^{n+1} \bar{c}_K^n$ in (5.4) and rearranging terms gives

$$\begin{aligned} & \left(\bar{s}_K^{n+1} + \frac{1-\varphi}{\varphi} \rho_r a'(\xi_K) \right) (\bar{c}_K^{n+1} - \bar{c}_K^n) + \bar{c}_K^n (\bar{s}_K^{n+1} - \bar{s}_K^n) \\ &= -\frac{\Delta t}{\varphi |K|} \sum_{e \in \partial K} \sum_{i=1}^q |e| \omega_i (\check{c}_{e,i} \hat{F}_{e,i}^+ + \hat{c}_{e,i} \hat{F}_{e,i}^-), \end{aligned}$$

where

$$a'(\xi_K) = \frac{a(\bar{c}_K^{n+1}) - a(\bar{c}_K^n)}{\bar{c}_K^{n+1} - \bar{c}_K^n} \quad \text{for some point } \xi_K \text{ between } \bar{c}_K^{n+1} \text{ and } \bar{c}_K^n.$$

We then proceed to replace $\bar{s}_K^{n+1} - \bar{s}_K^n$ by (5.1), leading to

$$\begin{aligned} & \left(\bar{s}_K^{n+1} + \frac{1-\varphi}{\varphi} \rho_r a'(\xi_K) \right) (\bar{c}_K^{n+1} - \bar{c}_K^n) + \bar{c}_K^n \left(-\frac{\Delta t}{\varphi |K|} \sum_{e \in \partial K} \sum_{i=1}^q \omega_i |e| (\hat{F}_{e,i}^+ + \hat{F}_{e,i}^-) \right) \\ &= -\frac{\Delta t}{\varphi |K|} \sum_{e \in \partial K} \sum_{i=1}^q |e| \omega_i (\check{c}_{e,i} \hat{F}_{e,i}^+ + \hat{c}_{e,i} \hat{F}_{e,i}^-), \end{aligned}$$

which can be written as

$$(5.12) \quad \bar{c}_K^{n+1} = \bar{c}_K^n - \frac{\Delta t}{\varsigma_K \varphi |K|} \sum_{e \in \partial K} \sum_{i=1}^q |e| \omega_i (\hat{F}_{e,i}^+ (\check{c}_{e,i} - \bar{c}_K^n) + \hat{F}_{e,i}^- (\hat{c}_{e,i} - \bar{c}_K^n)),$$

where $\varsigma_K := \bar{s}_K^{n+1} + (1-\varphi)\varphi^{-1}\rho_r a'(\xi_K) > 0$, since $\bar{s}_K^n \in [0,1]$ and $da/dc > 0$. Considering also the boundary terms, and using (5.5), we obtain from relation (5.12)

$$(5.13) \quad \begin{aligned} \bar{c}_K^{n+1} &= \bar{c}_K^n + \Delta t \sum_{e=K|L \in \partial K \setminus \partial \Omega} \sum_{i=1}^q (\eta_{e,i}^+ (-\bar{c}_{K,L,i}^n) + \eta_{e,i}^- (\bar{c}_{L,K,i}^n + \bar{c}_L^n - \bar{c}_K^n)) \\ &+ \Delta t \sum_{e \in \partial K \cap \partial \Omega} \sum_{i=1}^q (\eta_{e,i}^+ (-\bar{c}_{K,e,i}^n) + \eta_{e,i}^- (c_{e,i}^b - \bar{c}_K^n)), \end{aligned}$$

where

$$(5.14) \quad \eta_{e,i}^+ = \frac{|e| \omega_i \hat{F}_{e,i}^+}{\varsigma_K \varphi |K|} \geq 0, \quad \eta_{e,i}^- = -\frac{|e| \omega_i \hat{F}_{e,i}^-}{\varsigma_K \varphi |K|} \geq 0.$$

Then Lemma 5.5 allows us to write

$$\begin{aligned} -\check{c}_{K,L,i} &= \sum_{N \in \mathcal{N}_K} \theta_{K,L,N}^i (\Delta_{K,N}) + \sum_{d \in \partial K \cap \partial \Omega} \theta_{K,L,d}^i (\Delta_{K,d}), \\ \check{c}_{L,K,i} &= \sum_{N \in \mathcal{N}_K} \vartheta_{L,K,N}^i (\Delta_{K,N}) + \sum_{d \in \partial K \cap \partial \Omega} \vartheta_{L,K,d}^i (\Delta_{K,d}), \end{aligned}$$

where $\theta_{K,L,N}^i, \vartheta_{L,K,N}^i, \theta_{K,L,d}^i, \vartheta_{L,K,d}^i \geq 0$. Inserting these values into (5.13) leads to

$$(5.15) \quad \begin{aligned} \bar{c}_K^{n+1} = \bar{c}_K^n + \Delta t \sum_{N \in \mathcal{N}_K} \Theta_{K,N}(\Delta_{K,N}) + \Delta t \sum_{d \in \partial K \cap \partial \Omega} \Theta_{K,d}(\Delta_{K,d}) \\ + \Delta t \sum_{d \in \partial K \cap \partial \Omega} \sum_{i=1}^q \eta_{d,i}^- (c_{d,i}^b - \bar{c}_K^n), \end{aligned}$$

with

$$(5.16) \quad \begin{aligned} \Theta_{K,N} := & \sum_{e=K|L \in \partial K \setminus \partial \Omega} \sum_{i=1}^q (\eta_{e,i}^+ \theta_{K,L,N}^i + \eta_{e,i}^- \vartheta_{L,K,N}^i) + \sum_{d \in \partial K \cap \partial \Omega} \sum_{i=1}^q \eta_{d,i}^+ \theta_{K,d,N}^i \\ & + \sum_{i=1}^q \eta_{e_N,i}^-, \\ \Theta_{K,d} := & \sum_{e=K|L \in \partial K \setminus \partial \Omega} \sum_{i=1}^q (\eta_{e,i}^+ \theta_{K,L,d}^i + \eta_{e,i}^- \vartheta_{L,K,d}^i) + \sum_{\sigma \in \partial K \cap \partial \Omega} \sum_{i=1}^q \eta_{\sigma,i}^+ \theta_{K,\sigma,d}^i, \end{aligned}$$

where $e_N = K|N$. The following result gives a bound for Δt , valid whenever (5.11) holds and $\omega_i \geq 0$ for all i . Therefore, from (5.15) we conclude that (5.10) holds. \square

LEMMA 5.6. *Under the assumptions of Theorem 5.2 there holds*

$$\Upsilon_K := \Delta t \left(\sum_{N \in \mathcal{N}_K} \Theta_{K,N} + \sum_{d \in \partial K \cap \partial \Omega} \Theta_{K,d} + \sum_{d \in \partial K \cap \partial \Omega} \sum_{i=1}^q \eta_{d,i}^- \right) \leq 1 \quad \text{for all } K \in \mathcal{T}_h,$$

where $\Theta_{K,N}, \Theta_{K,d}$ and $\eta_{d,i}^-$ are given in (5.16) and (5.14), respectively.

Proof. For a given K , let $\mathcal{A} := \partial K \cap \partial \Omega$ and $\mathcal{B} := \partial K \setminus \partial \Omega$. We write

$$\begin{aligned} \Upsilon_K = \Delta t & \left(\sum_{N \in \mathcal{N}_K} \left\{ \sum_{\substack{e=K|L \in \mathcal{B} \\ i=1, \dots, q}} (\eta_{e,i}^+ \theta_{K,L,N}^i + \eta_{e,i}^- \vartheta_{L,K,N}^i) + \sum_{\substack{d \in \mathcal{A} \\ i=1, \dots, q}} \eta_{d,i}^+ \theta_{K,d,N}^i + \sum_{i=1}^q \eta_{e_N,i}^- \right\} \right. \\ & \left. + \sum_{d \in \mathcal{A}} \left\{ \sum_{\substack{e=K|L \in \mathcal{B} \\ i=1, \dots, q}} (\eta_{e,i}^+ \theta_{K,L,d}^i + \eta_{e,i}^- \vartheta_{L,K,d}^i) + \sum_{\substack{\sigma \in \mathcal{A} \\ i=1, \dots, q}} \eta_{\sigma,i}^+ \theta_{K,\sigma,d}^i \right\} + \sum_{\substack{d \in \mathcal{A} \\ i=1, \dots, q}} \eta_{d,i}^- \right) \\ \leq \text{cfl} & \left(\sum_{N \in \mathcal{N}_K} \left\{ \sum_{\substack{e=K|L \in \mathcal{B} \\ i=1, \dots, q}} \omega_i (\theta_{K,L,N}^i + \vartheta_{L,K,N}^i) + \sum_{\substack{d \in \mathcal{A} \\ i=1, \dots, q}} \omega_i \theta_{K,d,N}^i + \sum_{i=1}^q \omega_i \right\} \right. \\ & \left. + \sum_{d \in \mathcal{A}} \left\{ \sum_{\substack{e=K|L \in \mathcal{B} \\ i=1, \dots, q}} \omega_i (\theta_{K,L,d}^i + \vartheta_{L,K,d}^i) + \sum_{\substack{\sigma \in \mathcal{A} \\ i=1, \dots, q}} \omega_i \theta_{K,\sigma,d}^i \right\} + \sum_{\substack{d \in \mathcal{A} \\ i=1, \dots, q}} \omega_i \right). \end{aligned}$$

Finally, noting that $\sum_i \omega_i = 1$, we obtain

$$\begin{aligned}
\Upsilon_K &\leq \text{cff} \left(\sum_{\substack{e=K|L \in \mathcal{B} \\ i=1, \dots, q}} \omega_i 2\kappa\nu \sum_{N \in \mathcal{N}_K} 1 + \sum_{\substack{d \in \mathcal{A} \\ i=1, \dots, q}} \omega_i \kappa\nu \sum_{N \in \mathcal{N}_K} 1 + \sum_{N \in \mathcal{N}_K} 1 \right. \\
&\quad \left. + \sum_{\substack{e=K|L \in \mathcal{B} \\ i=1, \dots, q}} \omega_i 2\kappa\nu \sum_{d \in \mathcal{A}} 1 + \sum_{\substack{\sigma \in \mathcal{A} \\ i=1, \dots, q}} \omega_i \kappa\nu \sum_{d \in \mathcal{A}} 1 + \sum_{d \in \mathcal{A}} 1 \right) \quad \square \\
&\leq \text{cff} \left(\sum_{e=K|L \in \mathcal{B}} 6\kappa\nu + \sum_{e \in \mathcal{A}} 3\kappa\nu + 3 + \sum_{e=K|L \in \mathcal{B}} 4\kappa\nu + \sum_{e \in \mathcal{A}} 2\kappa\nu + 2 \right) \\
&\leq \text{cff}(18\kappa\nu + 6\kappa\nu + 3 + 12\kappa\nu + 4\kappa\nu + 2) \leq 1.
\end{aligned}$$

6. Numerical results. Before presenting the numerical tests, we recall that the interaction between the flow and transport solvers is realised using a classical iterative coupling (or sequential strategy). Starting from an initial saturation distribution, one solves first (1.3) for velocity and pressure, followed by a saturation/concentration solution which comprises an inner iteration loop to reduce the nonlinear residuals associated to the adsorption term. The Newton algorithm uses a relative tolerance of 10^{-5} . Additional fixed-point iterations of the local-in-time coupling are performed until a prescribed stopping criterion is met (based on the residuals and a tolerance of 10^{-6}), and then the algorithm advances to the next time step. In practice, no more than three Picard steps are required. All linear solves, including those inside the Newton steps, are performed using the distributed SuperLU method.

6.1. Spatio-temporal accuracy of transport and flow approximations.

In our first set of examples, we study the accuracy of the flow and transport solvers separately. First, regarding the flow approximation, if we assume a constant saturation and polymer concentration, we can construct the following closed-form solutions for the steady Brinkman problem

$$(6.1) \quad \mathbf{u}(x, y) = \begin{pmatrix} -256x^2(x-1)^2y(y-1)(2y-1) \\ 256y^2(y-1)^2x(x-1)(2x-1) \end{pmatrix}, \quad p(x, y) = \left(x - \frac{1}{2}\right) \left(y - \frac{1}{2}\right),$$

defined on the unit disk. Permeability and viscosity take constant values $\kappa = \mu = 1$, and \mathbf{g} is constructed inserting (6.1) in the momentum equation of (1.3). We choose the stabilisation parameter $\alpha = 2 \times 10^5$ and the mean value of the pressure approximation is fixed to zero using a real Lagrange multiplier. The convergence history associated to the scheme (3.3) is portrayed in Table 1, showing optimal convergence rates (of $O(h)$) measured in the energy norms (3.4).

Secondly, the accuracy of the approximate transport problem in case of smooth coefficients and regular solutions can be assessed through a convergence history generated using the following exact solution

$$s = \cos^2(\pi x) \cos^2(\pi y) \exp(-t), \quad c_l = 0.2l^2 + 0.025l \sin^2(\pi x) \sin^2(\pi y) \exp(-t),$$

for $l = 1, 2$ and defined on the unit disk, for $t \in [0, 1]$. A known velocity of the mixture is assumed $\mathbf{u} = (\sin(\pi x) \cos(\pi y), -\cos(\pi x) \sin(\pi y))^T \sin(t)$, and a set of adimensional parameters and nonlinear model functions closing the system is given by $\alpha = 10^3$, $f(s, \mathbf{c}) = s^2[s^2 + (1-s)^2(0.5 + 10c_1 + 5c_2)]^{-1}$, $a(c_l) = c_l(5 + 5c_l)^{-1}$, $k_{\text{rw}} = s^2$, $k_{\text{rn}} = (1-s)^2$, $\varphi = 1$, $\mu_{\text{w}}(c_1, c_2) = \mu_{\text{w},0} + \mu_{\text{w},0}(c_1 + c_2)$, $\mu_{\text{w},0} = 0.1$, $\mu_{\text{n}} = 1$, and $\kappa = 1$.

D.o.f.	h	$e_0(\mathbf{u})$	rate	$e_h(\mathbf{u})$	rate	$e_h(p)$	rate
84	0.4714	0.8044	–	6.8137	–	2.9578	–
220	0.2828	0.3443	1.8014	3.8800	0.8916	1.4863	0.9394
684	0.1571	0.1129	1.8522	2.2360	0.9376	0.6668	1.3638
2380	0.0832	0.0367	1.8996	1.1969	0.9827	0.2358	1.4343
8844	0.0429	0.0108	1.9239	0.6209	0.9896	0.1122	1.1202
34060	0.0218	0.0031	1.9711	0.3205	0.9853	0.0612	0.9854
133607	0.0110	0.0009	1.9821	0.1614	0.9864	0.0368	0.9918
529458	0.0055	0.0003	1.9944	0.0734	0.9933	0.0181	0.9985

TABLE 1

Test 1A: convergence history for the stabilised mixed DG method for the Brinkman flow equations using a $\mathbb{BDM}_1 - \mathbb{P}_0$ approximation of velocity and pressure.

To assess the convergence properties of the spatial DG discretisation, we choose a fine timestep $\Delta t = 10^{-3}$ and partition Ω into a sequence of eight successively refined meshes and measure errors in the energy norm for piecewise linear and piecewise quadratic approximations (i.e. $k = 1, 2$), computed at the final time $t = 1$. Table 2 indicates that the method achieves an asymptotic $O(h^k)$ convergence. The accuracy of the temporal optimal SSP-RK scheme (explicit, of three stages and of third order, using an effective SSP coefficient of $1/3$) is studied by setting a fine-resolution space discretisation with $h = 2^{-7}$ and successively refine the time interval on seven levels. For these smooth solutions, an optimal convergence order of $O(\Delta t^3)$ is obtained when measuring errors in the $\ell^\infty(H^1)$ -norm at $t = 0.5$, as presented in Figure 2. The use of more RK stages will produce smaller errors, but the convergence order will remain the same.

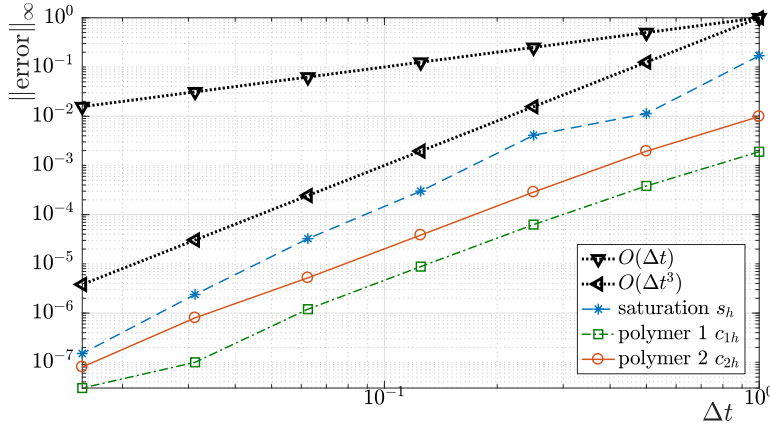


FIG. 2. Test 1C: error history associated to the time discretisation of the coupled system using a SSP-RK method of order 3.

6.2. Water-oil system. With the aim of testing the suitability of the method in the presence of rough coefficients and when sharp features are expected in the solution, let us now consider the infiltration of water into oil, first without the action of polymers, that is, we set $\mathbf{c} \equiv \mathbf{0}$. We conduct a classical simulation on a porous box $\Omega = (0, 1.4) \times (0, 1)$, with constant porosity $\varphi = 0.35$ and having an idealised winding crack of sinusoidal shape, characterised by the intrinsic permeability $\kappa(x, y) =$

D.o.f.	h	$e(s)$	rate	$e(c_1)$	rate	$e(c_2)$	rate
($k = 1$)							
18	2.0000	2.3284	–	0.7835	–	0.5116	–
54	1.0000	1.1266	0.9798	0.2998	1.3857	0.1415	1.1951
162	0.8854	0.9411	1.0778	0.1753	0.9514	0.0720	0.8478
558	0.5000	0.3521	1.0204	0.1275	1.0413	0.0361	0.9681
1890	0.2848	0.1258	1.0284	0.0961	0.9525	0.0196	0.9862
6732	0.1489	0.0406	1.0455	0.0584	0.9616	0.0101	0.9752
26946	0.0770	0.0215	0.9574	0.0301	0.9884	0.0060	0.9641
104634	0.0427	0.0153	0.9502	0.0188	0.9463	0.0032	0.9547
($k = 2$)							
36	2.0000	1.4722	–	0.4025	–	0.2599	–
108	1.0000	0.8280	1.4112	0.1832	1.5648	0.1258	1.8019
324	0.8854	0.2322	1.9733	0.0614	1.9634	0.0438	1.4250
1116	0.5000	0.1266	1.8991	0.0175	1.8773	0.0162	1.9081
3780	0.2848	0.0403	1.9802	0.0048	1.9678	0.0042	1.8655
13464	0.1489	0.0161	1.9753	0.0013	1.9471	0.0011	1.6568
53892	0.0770	0.0054	1.9276	0.0004	1.8612	0.0004	1.9523
209268	0.0427	0.0015	1.7427	0.0001	1.8951	0.0001	2.0091

TABLE 2

Test 1B: convergence history for the stabilised DG method (using piecewise linear and piecewise quadratic elements) for the transport equations. Errors are measured in the broken H^1 -norm.

$\max\{\exp(-10y + 5 + \sin(10x))^2, 0.01\}$. We employ the mildly nonlinear Brooks-Corey relative permeabilities $k_{rw} = s^2$, $k_{rn} = (1 - s)^2$, so the mobilities and fractional flow function (of the wetting phase) depend only on the water saturation. No gravity effects are taken into account, and the remaining model parameters are set as $\mu_w = 0.25$ and $\mu_n = 1$. We construct an unstructured triangular mesh of 45360 elements, and at each time iteration, the timestep is determined from a CFL condition, which in this case produces an average step of $\Delta t = 5 \times 10^{-4}$. The stabilisation parameter used here is $\alpha = 10^3$. The porous block is initially full of oil (that is, $s = 0$) and a constant profile of water ($s = 1$) is imposed on the left wall (which is the inflow boundary), a linear pressure profile $p_0(x, y) = (1.4 - x)/1.4$ is imposed on the whole boundary (and actually implemented as a natural boundary condition, with an additional term $-\langle p_0, \mathbf{v}_h \cdot \mathbf{n} \rangle_{\partial\Omega}$ appearing as part of the right hand side \mathcal{F}^s of the weak formulation (3.3)), and the velocity is not prescribed. It is stressed that a careful treatment of the numerical flux at the inflow boundary is essential to actually onset the injection of water into the domain. The system is evolved for about 1000 timesteps, and we collect the numerical results in Figure 3. Iso-contours of each individual field are displayed at two time instants, showing the expected advancing of the water front following the preferential path marked by the winding crack, and high velocity gradients on the region of large permeabilities.

6.3. Polymer flooding of an idealised reservoir. We now turn to the simulation of polymer flooding of an oil reservoir, where the full model specified in Section 2 is relevant. We consider $\mathcal{M} = 1$ and model parameters together with constitutive relationships (modified from those in [34]) are taken as follows: $a_1(\mathbf{c}) = a(c) = c_{\max} \frac{a_0 c}{1 + a_0 c}$, $\mu_w(c) = \mu_{w,0} + 0.75 \mu_{w,0} c_{\max}^{-1} c$, $\rho_w = 1$, $\rho_n = 0.58$, $\mu_w^0 = 0.35$, $\mu_n = 3.5$, $\varphi = 0.25$,

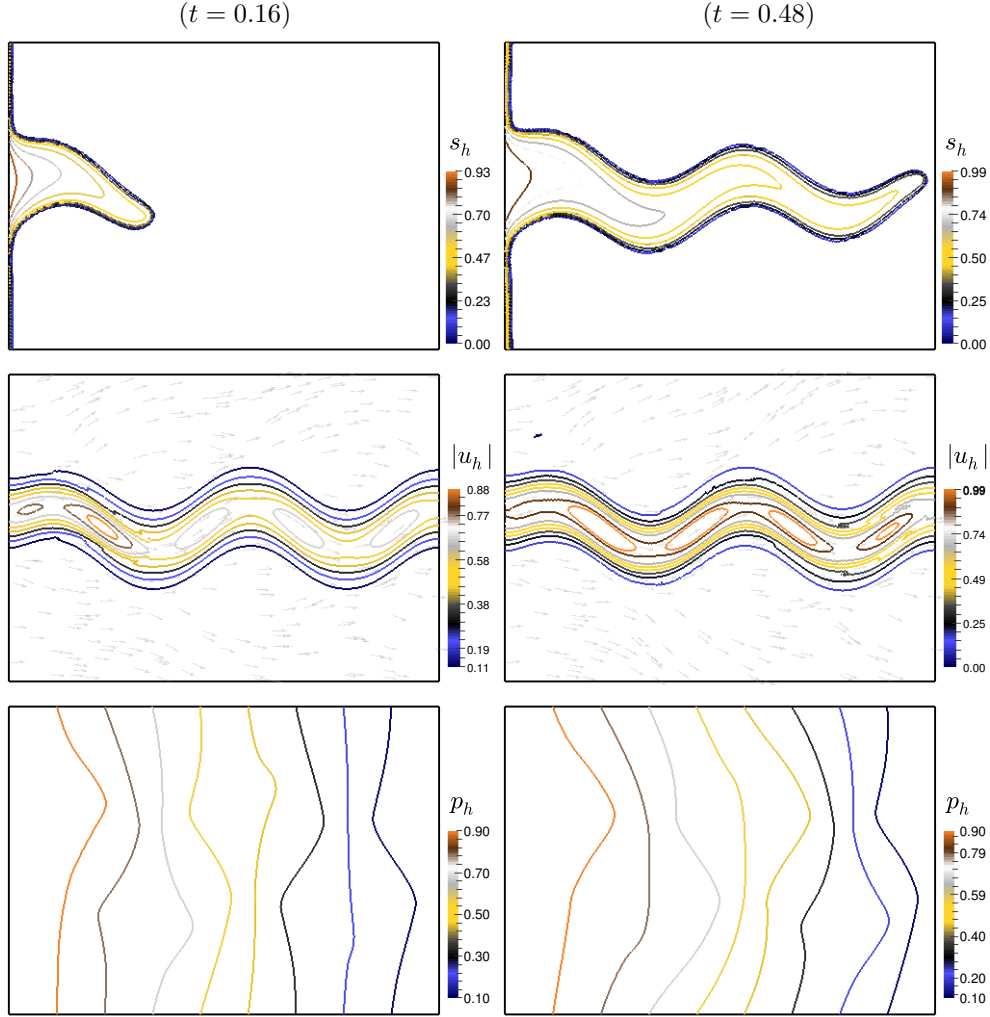


FIG. 3. Test 2: numerical solution of the water infiltration in porous media computed with a non-conforming Brezzi-Douglas-Marini approximation of velocity, and piecewise discontinuous saturation and pressure. Evolution of the water saturation (top), magnitude of the velocity field (middle panels) and pressure profiles (bottom).

$a_0 = 0.1$, $\lambda_w(s, c) = s^2/\mu_w(c)$, $\lambda_n(s) = (1 - s)^2/\mu_n$. The stabilisation constant is $\alpha = 1$ and the domain is now the unit square $\Omega = (0, 1)^2$. The heterogeneity in the medium is incorporated through the same sinusoidal absolute permeability profile from last section. A quadratic pressure profile is imposed in the form of a natural boundary condition and we regard the obtained simulated scenarios at three different time instants. We consider again that the porous slab is initially full of oil and a constant profile of water ($s = 1$) and polymers ($c_{\max} \in \{0.2, 3.2\}$) is injected on the left wall. The domain is divided into 32K triangular elements and from Figure 4 we can observe the differences between the sweeping process (of transporting the oleic phase from the inlet boundary to the outlet) according to the concentration of polymers present at the inlet boundary. We then proceed to modify the permeability distribution incorporating a non-homogeneous field where 25 disks of radius 0.005 and having

a much lower permeability, are randomly located in the domain. More precisely, we set $\kappa(x, y) = \max(\sum_{i=1}^{25} \exp[-\frac{1}{0.005}\{(x - q_x(i))^2 + (y - q_y(i))^2\}], 0.0001)$, where the random points are $(q_x(i), q_y(i))$. Moreover, the rock porosity is decreased $\varphi = 0.2$, the pressure profile imposed on the boundaries is now linear, and we now assume that the effect of the external motion of the flow patterns is due to the polymer concentration rather than the water saturation. In this case the numerical results imply that more oil is displaced in the presence of a higher polymer concentration (here we compare the cases of $c_{\max} \in \{0.22, 3.9\}$), but due to gravity the polymers will tend to get retained within the reservoir (see Figure 5).

Appendix: proof of Lemma 5.4. We present the proofs for (5.7) and (5.8) in the following lines. From (5.5), suppressing the dependence on t^n and using Lemma 5.2, we obtain

$$-\tilde{c}_{K,L,i}^n = -c_h(\tilde{\mathbf{x}}_i^e) + \bar{c}_K^n = -c_h(\tilde{\mathbf{x}}_i^e) + c_h(\mathbf{x}_K) + \mathcal{O}(h^2).$$

A Taylor expansion of c_h around \mathbf{x}_K now gives

$$\begin{aligned} -\tilde{c}_{K,L,i}^n &= -(\mathbf{x}_i^e - \mathbf{x}_K) \cdot \nabla c_h(\mathbf{x}_K) + \mathcal{O}(h^2) = -d_{K,L}^i \cdot \nabla c_h(\mathbf{x}_K) + \mathcal{O}(h^2) \\ (A.2) \quad &= (\theta_{K,L,M}^i d_{K,M} + \theta_{K,L,N}^i d_{K,N}) \cdot \nabla c_h(\mathbf{x}_K) + \mathcal{O}(h^2), \end{aligned}$$

and rearranging terms we get

$$d_{K,L} \cdot \nabla c_h(\mathbf{x}_K) = (\mathbf{x}_L - \mathbf{x}_K) \cdot \nabla c_h(\mathbf{x}_K) = c_h(\mathbf{x}_L) - c_h(\mathbf{x}_K) + \mathcal{O}(h^2), \quad L \in \mathcal{N}_K.$$

By Lemma 5.2, $c_h(\mathbf{x}_L) = \bar{c}_L + \mathcal{O}(h^2)$ for $L \in \mathcal{N}_K$; consequently,

$$d_{K,L} \cdot \nabla c_h(\mathbf{x}_K) = \bar{c}_L - \bar{c}_K + \mathcal{O}(h^2), \quad L \in \mathcal{N}_K.$$

Inserting these values into (A.2) we get

$$\begin{aligned} -\tilde{c}_{K,L,i}^n &= \theta_{K,L,M}^i (\bar{c}_M - \bar{c}_K + \mathcal{O}(h^2)) + \theta_{K,L,N}^i (\bar{c}_N - \bar{c}_K + \mathcal{O}(h^2)) + \mathcal{O}(h^2), \\ &= \theta_{K,L,M}^i \Delta_{K,M} + \theta_{K,L,N}^i \Delta_{K,N} + \mathcal{O}(h^2), \end{aligned}$$

which verifies (5.7). Since c_h is assumed smooth, $\tilde{c}_h(\tilde{\mathbf{x}}_i^e, t^n) = c_h(\tilde{\mathbf{x}}_i^e, t^n)$. Next, from (5.5) we can use similar arguments as above (namely a Taylor expansion of c_h around \mathbf{x}_K and Lemma 5.2 repeatedly) to obtain

$$\begin{aligned} \tilde{c}_{L,K,i}^n &= c_h(\tilde{\mathbf{x}}_i^e, t^n) - \bar{c}_L^n = c_h(\mathbf{x}_K) + (\mathbf{x}_i^e - \mathbf{x}_K) \cdot \nabla c_h(\mathbf{x}_K) - \bar{c}_L^n + \mathcal{O}(h^2) \\ &= \bar{c}_K^n + (\mathbf{x}_i^e - \mathbf{x}_L + \mathbf{x}_L - \mathbf{x}_K) \cdot \nabla c_h(\mathbf{x}_K) - \bar{c}_L^n + \mathcal{O}(h^2) \\ &= \bar{c}_K^n - \bar{c}_L^n + (c_h(\mathbf{x}_L) - c_h(\mathbf{x}_K)) + (\mathbf{x}_i^e - \mathbf{x}_L) \cdot \nabla c_h(\mathbf{x}_K) + \mathcal{O}(h^2) \\ &= \bar{c}_K^n - \bar{c}_{\mathbf{x}_i}^n + (\bar{c}_L - \bar{c}_K) + (\tilde{\mathbf{x}}_i^e - \mathbf{x}_L) \cdot \nabla c_h(\mathbf{x}_K) + \mathcal{O}(h^2) \\ &= \vartheta_{L,K,M}^i d_{K,M} \cdot \nabla c_h(\mathbf{x}_K) + \vartheta_{L,K,N}^i d_{K,N} \cdot \nabla c_h(\mathbf{x}_K) + \mathcal{O}(h^2). \end{aligned}$$

Using once again the Taylor expansion of c_h around the point B we get

$$d_{K,L} \cdot \nabla c_h(\mathbf{x}_K) = (\mathbf{x}_L - \mathbf{x}_K) \cdot \nabla c_h(\mathbf{x}_K) = c_h(\mathbf{x}_L) - c_h(\mathbf{x}_K) + \mathcal{O}(h^2), \quad L \in \mathcal{N}_K,$$

and as before, $d_{K,L} \cdot \nabla c_h(\mathbf{x}_K) = \bar{c}_L - \bar{c}_K + \mathcal{O}(h^2)$ for $L \in \mathcal{N}_K$. This finally leads to (5.8) in the following manner

$$\begin{aligned} \tilde{c}_{L,K,i}^n &= \vartheta_{L,K,M}^i (\bar{c}_M - \bar{c}_K + \mathcal{O}(h^2)) + \vartheta_{L,K,N}^i (\bar{c}_N - \bar{c}_K + \mathcal{O}(h^2)) + \mathcal{O}(h^2) \\ &= \vartheta_{L,K,M}^i \Delta_{K,M} + \vartheta_{L,K,N}^i \Delta_{K,N} + \mathcal{O}(h^2). \end{aligned}$$

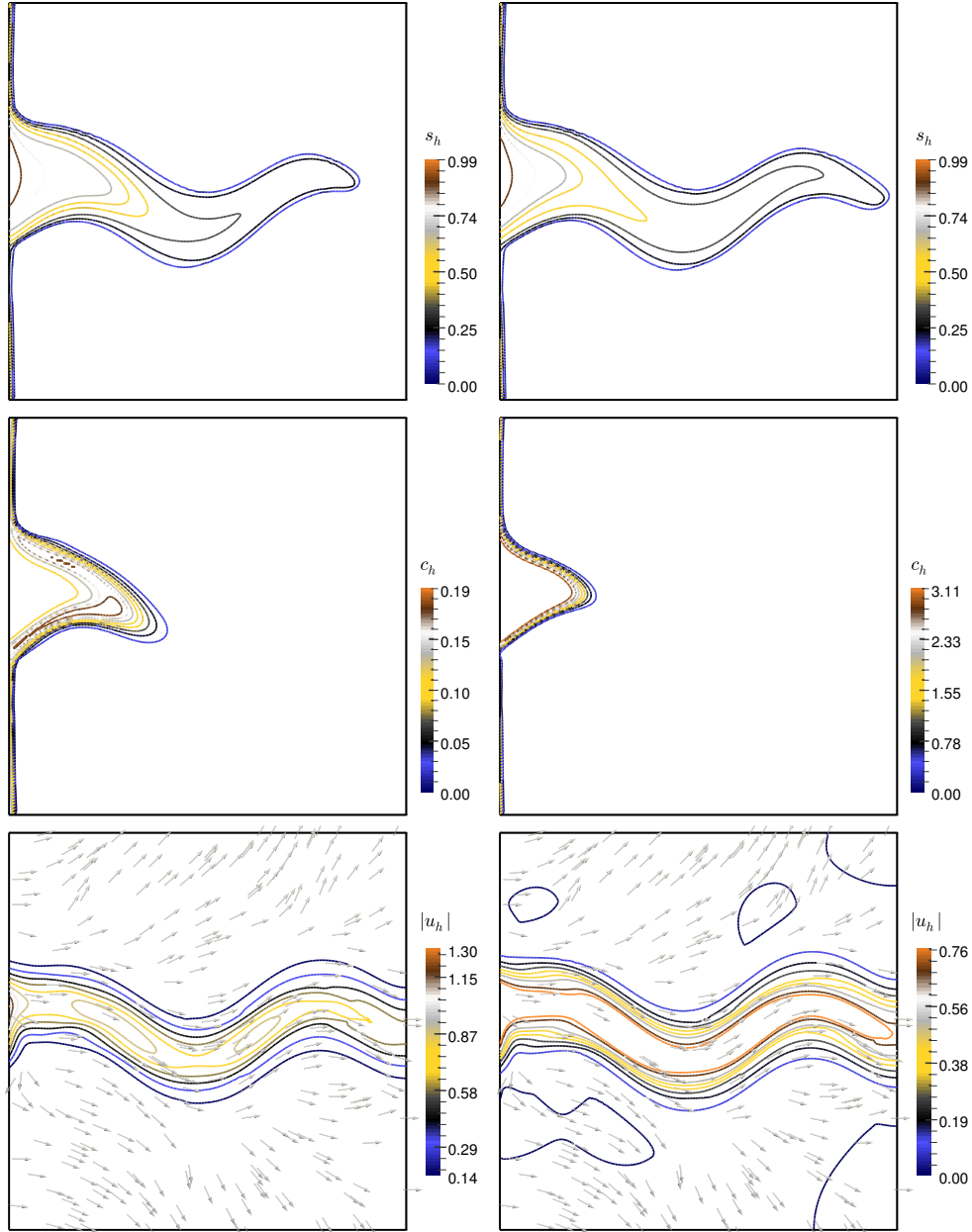


FIG. 4. Test 3A: snapshots at $t = 0.2$ of the saturation (top), polymer concentration (middle), and velocity profiles (bottom) obtained according to a low (left) and high (right) polymer concentration imposed at the inlet boundary.

REFERENCES

- [1] ADIMURTHI, J. JAFFRÉ, AND G. D. VEERAPPA GOWDA, *Godunov-type methods for conservation laws with a flux function discontinuous in space*, SIAM J. Numer. Anal., 42 (2004), pp. 179–208.
- [2] ADIMURTHI, G. D. VEERAPPA GOWDA, AND J. JAFFRÉ, *The DFLU flux for systems*

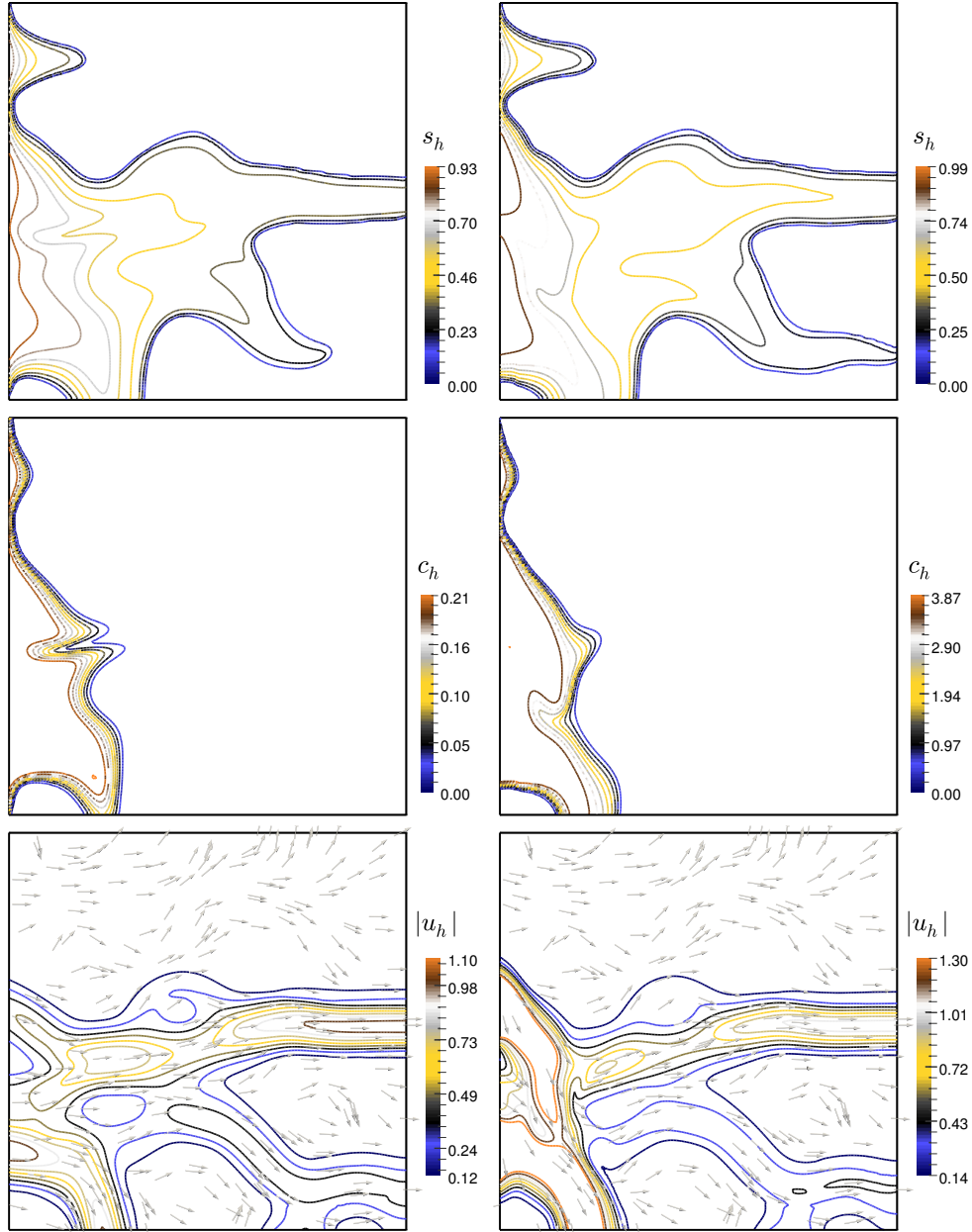


FIG. 5. Test 3B: snapshots at $t = 0.25$ of the saturation (top), polymer concentration (middle), and velocity profiles (bottom) obtained according to a low (left) and high (right) polymer concentration imposed at the inlet boundary.

- of conservation laws, *J. Comput. Appl. Math.*, 247 (2013), pp. 102–123.
- [3] L. BERGAMASCHI, S. MANTICA, AND G. MANZINI, *A mixed finite element-finite volume formulation of the black-oil model*, *SIAM J. Sci. Comput.*, 20 (1998), pp. 970–997.
- [4] F. BREZZI, J. DOUGLAS, AND L. D. MARINI, *Two families of mixed finite elements for second order elliptic problems*, *Numer. Math.*, 47 (1985), pp. 217–235.
- [5] H. C. BRINKMAN, *A calculation of the viscous force exerted by a flowing fluid on a*

- dense swarm of particles*, Appl. Sci. Res., A 1 (1947), pp. 27–34.
- [6] R. H. BROOKS AND A. T. COREY, *Hydraulic properties of porous media*, Hydrological Paper 3, (1964).
- [7] S. BUCKLEY AND M. LEVERETT, *Mechanism of fluid displacement in sands*, Trans. AIME, 146 (1942), pp. 107–116.
- [8] R. BÜRGER, S. KUMAR, S.K. KENETTINKARA, AND R. RUIZ-BAIER, *Discontinuous approximation of viscous two-phase flow in heterogeneous porous media*, J. Comput. Phys., 321 (2016), pp. 126–150.
- [9] R. BÜRGER, S. KUMAR, AND R. RUIZ-BAIER, *Discontinuous finite volume element discretization for coupled flow–transport problems arising in models of sedimentation*, J. Comput. Phys., 299 (2015), pp. 446–471.
- [10] R. BÜRGER, R. RUIZ-BAIER, AND H. TORRES, *A stabilized finite volume element formulation for sedimentation-consolidation processes*, SIAM J. Sci. Comput., 34 (2012), pp. B265–B289.
- [11] C. CALGARO, E. CREUSÉ, AND T. GOUDON, *An hybrid finite volume-finite element method for variable density incompressible flows*, J. Comput. Phys., 227 (2008), pp. 4671–4696.
- [12] B. COCKBURN, S. HOU, AND C.-W. SHU, *The Runge-Kutta local projection discontinuous Galerkin finite element method for conservation laws. IV. The multidimensional case*, Math. Comp., 54 (1990), pp. 545–581.
- [13] F. CRAIG, *The Reservoir Engineering Aspects of Water Flooding*, SPE of AIME, (1971).
- [14] T. Q. C. DANG, Z. CHEN, T. B. N. NGUYEN, AND W. BAE, *Investigation of isotherm polymer adsorption in porous media*, Pet. Sci. Technol., 32 (2014), pp. 1626–1640.
- [15] R.E. EWING, R.D. LAZAROV, AND Y. LIN, *Finite volume element approximations of nonlocal reactive flows in porous media*, Numer. Methods Partial Diff. Eqns., 16 (2000), pp. 285–311.
- [16] S. GOTTLIEB, D.I. KETCHESON, AND C.-W. SHU, *High order strong stability preserving time discretizations*, J. Sci. Comput., 38 (2009), pp. 251–289.
- [17] E. L. ISAACSON, *Global Solution of a Riemann Problem for a Non-strictly Hyperbolic System of Conservation Laws Arising in Enhanced Oil Recovery*, Enhanced Oil Recovery Institute, University of Wyoming, 1989.
- [18] E. L. ISAACSON AND J. B. TEMPLE, *Analysis of a singular hyperbolic system of conservation laws*, J. Differential Equations, 65 (1986), pp. 250–268.
- [19] T. JOHANSEN, A. TVEITO, AND R. WINTHER, *A Riemann solver for a two-phase multicomponent process*, SIAM J. Sci. Statist. Comput., 10 (1989), pp. 846–879.
- [20] T. JOHANSEN AND R. WINTHER, *The solution of the Riemann problem for a hyperbolic system of conservation laws modeling polymer flooding*, SIAM J. Math. Anal., 19 (1988), pp. 541–566.
- [21] T. JOHANSEN AND R. WINTHER, *The Riemann problem for multicomponent polymer flooding*, SIAM J. Math. Anal., 20 (1989), pp. 908–929.
- [22] C. KLINGENBERG AND N.H. RISEBRO, *Stability of a resonant system of conservation laws modeling polymer flow with gravitation*, J. Differential Equations, 170 (2001), pp. 344–380.
- [23] J. KÖNNÖ AND R. STENBERG, *$H(\text{div})$ -conforming finite elements for the Brinkman problem*, Math. Models Methods Appl. Sci., 21(11) (2011), pp. 2227–2248.
- [24] S. KUMAR, *A mixed and discontinuous Galerkin finite volume element method for incompressible miscible displacement problems in porous media*, Numer. Methods Partial Differential Equations, 28(4) (2012), pp. 1354–1381.
- [25] S. KUMAR, *On the approximation of incompressible miscible displacement problems in porous media by mixed and standard finite volume element methods*, Int. J. Model. Simul. Sci. Comput., 4(3) (2013), pp. 1–30.
- [26] M. OHLBERGER, *Convergence of a mixed finite element-finite volume method for the two phase flow in porous media*, East-West J. Numer. Math., 5 (1997), pp. 183–210.

- [27] S. OSHER AND C.-W. SHU, *Efficient implementation of essentially non-oscillatory shock-capturing schemes*, J. Comput. Phys., 77 (1988), pp. 439–471.
- [28] G. POPE, *The application of fractional flow theory to enhanced oil recovery*, Soc. Pet. Eng. J., 20 (1980), pp. 191–205.
- [29] H.-K. RHEE, R. ARIS, AND N.R. AMUNDSON, *First-Order Partial Differential Equations. Volume 2: Theory and Application of Hyperbolic Systems of Quasilinear Equations*, Prentice Hall, Englewood Cliffs, NJ, 1989.
- [30] D. RODRIGUEZ, L. ROMERO-ZERÓN, AND B. WEI, *Oil displacement mechanisms of viscoelastic polymers in enhanced oil recovery (EOR): a review*, J. Petrol. Explor. Prod. Technol., 4 (2014), pp. 113–121.
- [31] R. RUIZ-BAIER AND I. LUNATI, *Mixed finite element–discontinuous finite volume element discretization of a general class of multicontinuum models*, J. Comput. Phys., 322 (2016), pp. 666–688.
- [32] R. RUIZ-BAIER AND H. TORRES, *Numerical solution of a multidimensional sedimentation problem using finite volume-element methods*, Appl. Numer. Math., 95 (2015), pp. 280–291.
- [33] K. S. SCHMID, S. GEIGER, AND K. S. SORBIE, *Higher order FE–FV method on unstructured grids for transport and two-phase flow with variable viscosity in heterogeneous porous media*, J. Comput. Phys., 241 (2013), pp. 416–444.
- [34] K. SUDARSHAN KUMAR, C. PRAVEEN, AND G. D. VEERAPPA GOWDA, *A finite volume method for a two-phase multicomponent polymer flooding*, J. Comput. Phys., 275 (2014), pp. 667–695.
- [35] A. TVEITO AND R. WINTHER, *The solution of nonstrictly hyperbolic conservation laws may be hard to compute*, SIAM J. Sci. Comput., 16 (1995), pp. 320–329.
- [36] J. WEGNER AND L. GANZER, *Numerical simulation of oil recovery by polymer injection using COMSOL*, Proceedings of the 2012 COMSOL conference.
- [37] J. WHITELEY, *A discontinuous Galerkin finite element method for multiphase viscous flow*, SIAM J. Sci. Comput., 37 (2015), pp. B591–B612.

Centro de Investigación en Ingeniería Matemática (CI²MA)

PRE-PUBLICACIONES 2016 - 2017

- 2016-39 RAIMUND BÜRGER, STEFAN DIEHL, MARÍA CARMEN MARTÍ, PEP MULET, INGOMAR NOPENS, ELENA TORFS, PETER VANROLLEGHEM: *Numerical solution of a multi-class model for batch settling in water resource recovery facilities*
- 2016-40 RAIMUND BÜRGER, JULIO CAREAGA, STEFAN DIEHL: *Flux identification for scalar conservation laws modelling sedimentation in vessels with varying cross-sectional area*
- 2016-41 CHRISTOPHE CHALONS, PAOLA GOATIN, LUIS M. VILLADA: *High order numerical schemes for one-dimension non-local conservation laws*
- 2016-42 JESSIKA CAMAÑO, CHRISTOPHER LACKNER, PETER MONK: *Electromagnetic Stekloff eigenvalues in inverse scattering*
- 2017-01 RAIMUND BÜRGER, SUDARSHAN K. KENETTINKARA, DAVID ZORÍO: *Approximate Lax-Wendroff discontinuous Galerkin methods for hyperbolic conservation laws*
- 2017-02 DAVID MORA, GONZALO RIVERA, IVÁN VELÁSQUEZ: *A virtual element method for the vibration problem of Kirchhoff plates*
- 2017-03 CARLOS GARCIA, GABRIEL N. GATICA, ANTONIO MARQUEZ, SALIM MEDDAHI: *A fully discrete scheme for the pressure-stress formulation of the time-domain fluid-structure interaction problem*
- 2017-04 LUIS F. GATICA, FILANDER A. SEQUEIRA: *A priori and a posteriori error analyses of an HDG method for the Brinkman problem*
- 2017-05 ERNESTO CÁCERES, GABRIEL N. GATICA, FILANDER A. SEQUEIRA: *A mixed virtual element method for quasi-Newtonian Stokes flows*
- 2017-06 CELSO R. B. CABRAL, LUIS M. CASTRO, CHRISTIAN E. GALARZA, VÍCTOR H. LACHOS: *Robust quantile regression using a generalized class of skewed distributions*
- 2017-07 RAIMUND BÜRGER, JULIO CAREAGA, STEFAN DIEHL: *A simulation model for settling tanks with varying cross-sectional area*
- 2017-08 RAIMUND BÜRGER, SUDARSHAN K. KENETTINKARA, RICARDO RUIZ-BAIER, HECTOR TORRES: *Non-conforming/DG coupled schemes for multicomponent viscous flow in porous media with adsorption*

Para obtener copias de las Pre-Publicaciones, escribir o llamar a: DIRECTOR, CENTRO DE INVESTIGACIÓN EN INGENIERÍA MATEMÁTICA, UNIVERSIDAD DE CONCEPCIÓN, CASILLA 160-C, CONCEPCIÓN, CHILE, TEL.: 41-2661324, o bien, visitar la página web del centro: <http://www.ci2ma.udec.cl>



**CENTRO DE INVESTIGACIÓN EN
INGENIERÍA MATEMÁTICA (CI²MA)
Universidad de Concepción**



Casilla 160-C, Concepción, Chile
Tel.: 56-41-2661324/2661554/2661316
<http://www.ci2ma.udec.cl>

